A comparative analysis of the vestibular apparatus in Epipliopithecus vindobonensis: Phylogenetic implications

Alessandro Urciuoli, Clément Zanolli, Amélie Beaudet, Marta Pina, Sergio Almécija, Salvador Moyà-Solà, David M. Alba

A comparative analysis of the vestibular apparatus in *Epipliopithecus vindobonensis*: Phylogenetic implications

Alessandro Urciuoli [a,*], Clément Zanolli [b], Amélie Beaudet a, [c,d,a], Marta Pina [a,e], Sergio Almécija [f,g,a], Salvador Moyà-Solà [a,h,i], David M. Alba [a,*]

[a] *Institut Català de Paleontologia Miquel Crusafont, Universitat Autònoma de Barcelona, Edifici ICTA-ICP, c/ Columnes s/n, Campus de la UAB, 08193 Cerdanyola del Vallès, Barcelona, Spain*

[b] *Univ. Bordeaux, CNRS, MCC, PACEA, UMR 5199, F-33600 Pessac, France*

[c] *School of Geography, Archaeology and Environmental Studies, University of the Witwatersrand, Private Bag 3, Johannesburg, WITS 2050, South Africa*

[d] *Department of Anatomy, University of Pretoria, PO Box 2034, Pretoria, 0001, South Africa*

[e] *School of Earth and Environmental Sciences, Faculty of Science and Engineering, University of Manchester, 176 Oxford Road, Manchester M13 9PL, UK*

[f] *Division of Anthropology, American Museum of Natural History, Central Park West at 79th Street, New York, NY 10024, USA*

[g] *New York Consortium in Evolutionary Primatology, New York, NY, USA*

[h] *Institució Catalana de Recerca i Estudis Avançats (ICREA), Passeig de Lluís Companys 23, 08010 Barcelona, Spain*

[i] *Unitat d'Antropologia (Departament de Biologia Animal, Biologia Vegetal i Ecologia), Universitat Autònoma de Barcelona, Campus de la UAB s/n, 08193 Cerdanyola del Vallès, Barcelona, Spain*

*Corresponding authors.

E-mail address: alessandro.urciuoli@icp.cat (A. Urciuoli); david.alba@icp.cat (D.M. Alba).

[3] Department of Archaeology, University of Cambridge, Fitzwilliam St, Cambridge CB2 1QH, UK.

Abstract

Pliopithecoids are an extinct group of catarrhine primates from the Miocene of Eurasia. More than fifty years ago, they were linked to hylobatids due to some morphological similarities, but most subsequent studies have supported a stem catarrhine status, due to the retention of multiple plesiomorphic features (e.g., the ectotympanic morphology) relative to crown catarrhines. More recently, some morphological similarities to hominoids have been noted, raising the question of whether they could be stem members of this clade. To re-evaluate these competing hypotheses, we examine the morphology of the semicircular canals of the bony labyrinth of the middle Miocene pliopithecid *Epipliopithecus vindobonensis*. The semicircular canals are suitable to test between these hypotheses because: (1) they have been shown to embed strong phylogenetic signal and reliably discriminate among major clades; (2) several potential hominoid synapomorphies have been identified previously in the semicircular canals; and (3) semicircular canal morphology has not been previously described for any pliopithecoid. We use a deformation-based (landmark-free) three-dimensional geometric morphometric approach to compare *Epipliopithecus* with a broad primate sample of extant and extinct anthropoids. We quantify similarities in semicircular canal morphology using multivariate analyses, reconstruct ancestral morphotypes by means of a phylomorphospace approach, and identify catarrhine and hominoid synapomorphies based on discrete characters. *Epipliopithecus* semicircular canal morphology most closely resembles that of platyrrhines and *Aegyptopithecus* due to the retention of multiple anthropoid symplesiomorphies. However, *Epipliopithecus* is most parsimoniously interpreted as a stem catarrhine more

derived than *Aegyptopithecus* due to the possession of a crown catarrhine synapomorphy (i.e., the rounded anterior canal), combined with the lack of other catarrhine and any hominoid synapomorphies. Some similarities with hylobatids and atelids are interpreted as homoplasies likely related to positional behavior. The semicircular canal morphology of *Epipliopithecus* thus supports the common view that pliopithecoids are stem catarrhines.

Keywords: Pliopithecidae; Catarrhini; Miocene; Inner ear; Phylogeny; Geometric morphometrics

1. Introduction

1.1. The phylogenetic position of pliopithecoids

Pliopithecoids are an extinct superfamily of catarrhine primates, recorded in Eurasia from the early to the late Miocene (Andrews et al., 1996; Begun, 2002, 2017; Harrison, 2005, 2013). Their first occurrence, in the early Miocene of China (~18–17 Ma; Harrison and Gu, 1999; Begun, 2002; Harrison, 2013), slightly predates the oldest record of large-bodied apes in Eurasia (Heizmann and Begun, 2001; Casanovas-Vilar et al., 2011). In the absence of older (earliest Miocene) catarrhines in that continent, pliopithecoids are assumed to have an African origin (Harrison, 1987, 2013; Begun, 2017). Like apes, pliopithecoid ancestors probably dispersed into Eurasia before the Langhian transgression, which was possible due to the lowered sea level and tectonic events that led to the closure of the Tethys Seaway and the establishment of an intermittent terrestrial corridor beginning at ~19 Ma (Harzhauser et al., 2007; Harrison, 2013).

Decades ago, pliopithecoids were considered to be phylogenetically related to hylobatids due to some superficial resemblances in cranial morphology as well as body size and proportions (e.g., Hürzeler, 1954; Zapfe, 1958, 1960, 1961; Simons and Fleagle, 1973). Currently, they are generally considered a clade of stem catarrhines—as supported

by the retention of several cranial and postcranial features that are plesiomorphic compared to the crown members of the group (Andrews, 1975; Ciochon and Corruccini, 1977; Fleagle, 1984; Harrison, 1987, 2005, 2013; Andrews et al., 1996; Begun, 2002, 2017). The divergence of pliopithecoids before the split of crown catarrhines is further supported by most recent cladistic analyses (Zalmout et al., 2010; Stevens et al., 2013; Nengo et al., 2017; Gilbert et al., 2020), implying a long ghost lineage of ca. 12–14 Myr for pliopithecoids (Begun, 2017). The exception is the cladistic analysis by Alba et al. (2015), which recovered pliopithecoids as a clade of stem hominoids—thereby eliminating the need to hypothesize a long gap in the pliopithecoid fossil record. Most recently, Almécija et al. (2019) further documented similarities in femoral morphology between pliopithecoids (*Epipliopithecus*) and extant hominoids, thereby casting additional doubts on the status of pliopithecoids as stem catarrhines. Further uncertainty in this regard stems from the fact that no tail vertebrae are known from pliopithecoids (Begun, 2017). Based on sacral morphology, Zapfe (1958, 1961) argued that no external tail would have been present, as in hominoids; although this has subsequently been rebutted (Ankel, 1965; Russo, 2016), available evidence in this regard remains uncertain.

There are multiple genera of pliopithecids (Harrison and Gu, 1999; Moyà-Solà et al., 2001; Begun, 2002, 2017; Harrison, 2005, 2013; Alba et al., 2010; Alba and Moyà-Solà, 2012; Alba and Berning, 2013; Sankhyan et al., 2017; Harrison et al., 2020), which, following Harrison et al. (2020), we provisionally group into four different families: dionysopithecids (*Dionysopithecus* and *Platodontopithecus*), krishnapithecids (*Krishnapithecus*), pliopithecids (*Pliopithecus* and *Epipliopithecus*), and crouzeliids (*Plesiopliopithecus*, *Barberapithecus*, *Anapithecus*, *Egarapithecus*, and *Laccopithecus*). However, it is noteworthy that the treatment of these genera at the family rank, and even the placing of some genera in one or another group, differs among authors (e.g., compare Alba and Moyà-Solà, 2012 with Begun, 2017). Such disagreements largely stem from the

fact that the internal phylogeny of pliopithecoids is still unclear and that their affinities with fossil catarrhines from Africa remain uncertain (e.g., Harrison, 2013).

1.2. Evidence from Epipliopithecus

Deciphering the phylogenetic relationships of most pliopithecoids is hampered by the fact that they are mostly known by fragmentary dentognathic remains, with the exception of *Epipliopithecus vindobonensis*, whose craniodental and postcranial morphology is well documented by several skeletons from the middle Miocene (MN6, ~14.85–13.45 Ma[1]) karstic infillings of Devínska Nová Ves, Slovakia (Zapfe, 1958, 1961; Andrews et al., 1996; Begun, 2002; Harrison, 2013). *Epipliopithecus* was originally established as a subgenus of *Pliopithecus* by Zapfe and Hürzeler (1957), being subsequently considered a junior subjective synonym of the latter (e.g., Andrews et al., 1996; Harrison and Gu, 1999; Moyà-Solà et al., 2001; Harrison, 2005, 2013; Alba et al., 2010) or a distinct genus (e.g., Begun, 2002; Alba and Moyà-Solà, 2012; Arias-Martorell et al., 2015; Alba et al., 2015; this study). From a locomotor viewpoint, *E. vindobonensis* has been variously depicted as an arboreal or semiterrestrial generalized quadruped with varying degrees of climbing and suspensory abilities (see discussion in Arias-Martorell et al., 2015). From a phylogenetic perspective, its purported stem catarrhine status has been supported by features such as the short and only partially enclosed ectotympanic, the presence of entepicondylar foramen in the distal humerus, and single hinge-like carpometacarpal joint in the thumb (Zapfe, 1961; Szalay and Delson, 1979; Harrison, 1987, 2005; Andrews et al., 1996; Begun, 2002, 2017).

[1] Age uncertainly based on the boundaries recognized for MN6 (van der Meulen et al., 2011).

The external morphology of the petrosal bone of *E. vindobonensis* (Zapfe, 1961; Szalay, 1975; Fricano, 2018) has been of utmost significance in the discussion of its phylogenetic affinities, given that the presence of a tubular ectotympanic is considered synapomorphic of crown catarrhines (e.g., Szalay, 1975; Szalay and Delson, 1979; Harrison, 1987, 2005; Andrews et al., 1996; Begun, 2002; Zalmout et al., 2010; Alba et al., 2015; Nengo et al., 2017). The possibility remains that such ossification took place to some extent independently in cercopithecoids, hominoids and/or other anthropoids such as pliopithecoids (Begun, 2002, 2017; Alba et al., 2015). However, other features of *Epipliopithecus* also appear plesiomorphic as compared to crown catarrhines and show no particular similarities with hominoids, namely: the large postglenoid process separated from the acoustic meatus, as in platyrrhines (Zapfe, 1961); the lack of ossification in the tentorium cerebelli (unlike in most platyrrhines and stem anthropoids, but similar to *Aegyptopithecus* and crown catarrhines; Kay et al., 2009a); and the deep subarcuate fossa (Zapfe, 1961), as in platyrrhines and most anthropoids except hominids (Gannon et al., 1988; Kunimatsu et al., 2019). In contrast, the inner ear morphology of *Epipliopithecus* has not been described and therefore its potential phylogenetic implications remain unexplored.

1.3. The bony labyrinth of the inner ear

Among the inner cavities of the petrosal, the bony labyrinth of the inner ear is constituted by the semicircular canals (SCs) and the vestibule (which together host the soft-tissue structures linked with the sense of balance) plus the cochlea. Semicircular canal size (e.g., Spoor et al., 2007; Silcox et al., 2009; Ryan et al., 2012; Grohé et al., 2018) and orientation (David et al., 2010; Malinzak et al., 2012; Berlin et al., 2013; Perier et al., 2016; Gonzales et al., 2019) have been frequently used for inferring agility, while the shape of the canals as a whole has tentatively been linked to positional behavior (Le

153 Maître et al., 2017). At the same time, recent studies have demonstrated that the SCs bear
154 strong phylogenetic signal among anthropoids (Lebrun, 2010, 2012; Urciuoli et al., 2019,
155 2020; del Rio et al., 2020; Morimoto et al., 2020) and other mammals (e.g., Grohé et al.,
156 2015; Mennecart et al., 2016, 2017; Costeur et al., 2018).

157 Although adaptively relevant characters may constitute synapomorphies of
158 particular clades, arguably their relationship with function makes them potentially more
159 prone to homoplasy. However, the correlation between SC morphology and positional
160 behavior has recently been questioned by some studies (i.e., Rae et al., 2016; del Río et
161 al., 2020; Morimoto, et al., 2020), and SC shape variation has been shown to largely follow
162 the expectations of a Brownian motion mode of evolution in both platyrrhines (del Río et
163 al., 2020) and catarrhines (Urciuoli et al., 2020). These results are in accordance with
164 those obtained for the bony labyrinth as a whole, showing that its morphology reflects
165 phylogenetic relatedness as inferred from molecular data (Lebrun et al., 2010; Ekdale,
166 2013; Macrini, et al., 2013; Billet et al., 2015). Cumulatively, this evidence suggests that
167 bony labyrinth morphology is phylogenetically informative among mammals (Mennecart et
168 al., 2017) and may thus potentially illuminate the phylogenetic relationships of extinct
169 primates. Following Mennecart and Costeur (2016), who suggested that inner ear
170 structures might be highly informative for large cladistics analyses, Urciuoli et al. (2020)
171 explored catarrhine SC shape variation among catarrhines and proposed several potential
172 synapomorphies for crown hominoids.

173 Here we test between two different phylogenetic hypotheses for *Epipliopithecus*,
174 one hypothesis being that *Epipliopithecus* is a stem catarrhine, the other hypothesis that
175 *Epipliopithecus* is a hominoid, based on the information provided by the shape of the SCs
176 and vestibule. This morphology is described here for the first time using a three-
177 dimensional geometric morphometric (3DGM) approach applied to a broad sample of
178 extant and fossil anthropoids (Urciuoli et al., 2020). We refrained from analyzing the entire

bony labyrinth (i.e., including also the cochlea) because its potential for phylogenetic reconstruction among primates is currently unclear. A recent analysis in platyrrhines suggested that cochlear shape departs from a Brownian motion mode of evolution (Blomberg's K < 1; del Río et al., 2020), thus potentially reflecting a greater influence of function (and likely homoplasy due to similar selection pressures) than is the case for the SCs and vestibule. This is in agreement with previous studies linking several macroscopic cochlear features to hearing capabilities (e.g., Manoussaki et al., 2006; Kirk and Gosselin-Ildari, 2009; Coleman and Colbert, 2010). More detailed morphometric analyses of this structure among anthropoids is thus required to determine whether cochlear morphology can be meaningfully used to decipher the phylogenetic relationships of extinct catarrhines such as *Epipliopithecus*.

2. Materials and methods

2.1. Described material

We inspected three petrosals of *E. vindobonensis* belonging to two individuals from Devínska Nová Ves, Slovakia (Zapfe, 1960, 1961): NMB OE 303a, b (individual III), left (a) and right (b), housed in the Naturhistorisches Museum of Basel, Switzerland[2]; and NHMW 1970/1397/0003 (individual II), right, housed in the Naturhistorisches Museum of Wien, Austria.

2.2. Comparative sample

The comparative sample includes µCT scans of 162 dried crania and temporal bones belonging to 31 extant anthropoid species (see Supplementary Online Material [SOM] Table S1 for the sample size of the extant species), plus five fossil anthropoids

[2] Morimoto et al. (2020) included the bony labyrinth of NMB OE 303a in their comparative study but did not depict or specifically describe its morphology.

(SOM Table S2): the stem anthropoid *Parapithecus* (Bush et al., 2004), the stem catarrhine *Aegyptopithecus* (Simons et al., 2007), the stem platyrrhines *Dolichocebus* (Kay et al., 2009b) and *Homunculus* (Fulwood et al., 2016), and the hominoid *Oreopithecus* (Rook et al., 2004).

2.3. *Sample preparation*

NMB OE 303 was scanned with a Phoenix Nanotom®, GE at the Biomaterials Science Centre of the University of Basel (Switzerland) obtaining a voxel size of 25 µm. NHMW 1970/1397/0003 was scanned at the Vienna µCT-Lab using a Viscom X8060 (Viscom XT9190-THP X-ray tube) obtaining a voxel size of 22 µm. The canals and vestibule of NMB OE 303a, b were filled with air, while in NHMW 1970/1397/0003 they were partially filled with sediment. In both cases we segmented the SCs and vestibule cavities using the 'watershed' tool of Avizo v. 9.0.1 (FEI Visualization Sciences Group, Houston), with additional manual corrections for NHMW 1970/1397/0003. The 3D surfaces of NMB OE 303b and NHMW 1970/1397/0003 were mirrored for comparison. The 3D meshes of the two individuals are available from MorphoSource (see Table 1).

The µCT scans of most extant comparative species and of fossil anthropoids were accessed from MorphoSource.org digital repository (https://www.morphosource.org) with the exception of *Oreopithecus bambolii* petrosal, which was kindly provided by Lorenzo Rook (see SOM Table S2 for voxel sizes). Further details about the µCT scans of the extant comparative sample (voxel sizes, exact source, DOI, etc.) can be found in Urciuoli et al. (2020: Supplementary File 1). The slice stacks of these crania were processed using Avizo v. 9.0.1. and the left bony labyrinth was segmented using the semiautomatic 'watershed' tool of Avizo (with additional manual corrections in the case of partially filled canals found in the fossil specimens) and digitally extracted; when the left bony labyrinth was unavailable, the right one was mirrored. As in Urciuoli et al. (2020), the SCs and the

vestibule were separated from the cochlea by cutting the generated 3D meshes immediately inferior to the saccule and the oval window, using landmarks placed along the maximum curvature of the junction between the vestibule and the cochlea as reference for the cutting plane (Fig. 1). The resulting holes were filled with a flat surface using Geomagic Studio v. 2014.3.0 (3D Systems, Rock Hill, USA). Prior to the 3DGM analysis, the surfaces were first roughly prealigned by manually superimposing the meshes to ensure biological correspondence. Subsequently, the alignment was automatically refined using the Avizo module 'Align Surface' with the 'rigid + uniform' option. Similar to Procrustes superimposition, this module minimizes the distances between the faces of each surface by scaling, translating and rotating the analyzed meshes. The phylogenetic relationships of the extinct taxa included in the analyses, relative to extant anthropoids, are summarized in Figure 2.

2.4. Shape analysis

Differences in vestibule and SC shape were evaluated using a landmark-free 3DGM technique based on deformation, which relies on the geometrical correspondence of continuous surfaces and computes the magnitude and direction of deformation of the analyzed meshes from a group-average template (Glaunès and Joshi, 2006; Durrleman et al., 2012a, b; Dumoncel et al., 2014; Beaudet et al., 2016; Urciuoli et al., 2020). The deformations are mathematically modeled to obtain a one-to-one correspondence of the 3D space using the open-source software Deformetrica 4 (Bône et al., 2018). This technique yields results similar to landmark-based 3DGM methods while more easily tracking changes in volume (Urciuoli et al., 2020), and is less prone to biases introduced by the design of landmarking protocols, caused by the inherent difficulty to adequately capture complex 3D shapes based on a reduced number of homologous landmarks.

Due to the high computational power required, the sets of vectors, representing the flow of deformations from the initial position of the control points on the template to the target shape, were computed in the Barcelona Supercomputing Center (BSC) using the MinoTauro cluster (https://www.bsc.es/marenostrum/minotauro). To identify major patterns of shape variation across the sample, the resulting sets of vectors were inspected using between-group principal component analysis (bgPCA; Mitteroecker and Bookstein, 2011), using major clades (platyrrhines, cercopithecoids, hylobatids, and hominids) as the grouping factor (Urciuoli et al., 2020). To address recent concerns about the use of bgPCA based on highly multivariate data sets, such as those generated by 3DGM, and to rule out the presence of spurious groupings in our results (Bookstein, 2019; Cardini, et al., 2019), we computed cross-validated bgPCA scores. These were obtained by iteratively repeating the bgPCA on a subset of the sample. The cross-validated bgPCA scores were then compared to those obtained with standard bgPCA (Cardini and Polly, 2020). The affinities of fossil specimens with the groups defined a priori in the bgPCA were evaluated using the 'typprobClass' function of the Morpho package v. 2.7 (Schlager, 2017) in R v. 3.6.1 (R Core Team, 2019). This function computes posterior probabilities of group membership based on the Mahalanobis distances between the bgPC scores of fossil specimens and group centroids. Null hypotheses of group membership were rejected at $p < 0.05$. Similarities among anthropoid species were also evaluated by running a cluster analysis (Ward's method) on the Mahalanobis distances between pairs of bgPCA species centroid scores using the 'ward.D2' method of the 'hclust' function of the 'stats' package in R. The cophenetic correlation coefficient, which allows one to evaluate how faithfully the obtained dendrogram preserves the pairwise distances between the original unmodeled datapoints, was calculated using the same package.

In addition, we inspected the volumetric proportions of *Epipliopithecus* and the remaining fossil taxa included in the analysis, and determined the correlation between log-

transformed cube root canal volume (ln VolSC, mm) and log-transformed canal length (ln L, mm) by means of ordinary least-squares regression. Given that previous analyses identified an allometric grade shift between hominids and nonhominid anthropoids (Urciuoli et al., 2020), separate regression lines were computed for hominids and nonhominid anthropoid taxa using the 'stats' package in R.

2.5. Phylomorphospace, ancestral state estimation, and phylogenetic signal

To intuitively visualize the direction and magnitude of evolutionary change we relied on a phylomorphospace approach (Sidlauskas, 2008), by which a phylogenetic tree is projected onto the tangent space defined by the bgPCA of our shape data. Ancestral states for the internal nodes are estimated using a maximum likelihood method for continuous characters via the 'fastAnc' function of the 'phytools' version 0.6-60 package for R (Revell, 2012), while the tips of the tree branches correspond to the centroid scores for the included taxa. We repeated the analyses using two composite phylogenetic trees, one with *Epipliopithecus* as a stem catarrhine and the other with this taxon as a stem hominoid (Figs. 2 and 3). For extant taxa we relied on a Bayesian phylogenetic analysis of eleven mitochondrial and six autosomal genes downloaded from the 10kTrees Website v. 3 (Arnold et al., 2010). Extinct species were added based on their phylogenetic position, their divergence being arbitrarily placed 1 Myr before the estimated divergence age of the next derived node, and tip ages based on their chronostratigraphic age. We used the following tip age estimates: *Epipliopithecus* 14.15 Ma (mean of 14.85 and 13.45 Ma, the maximum-minimum age range for MN6 in central Europe according to van der Meulen et al., 2011); *Aegyptopithecus* and *Parapithecus*, 29.85 Ma (mean of 30.2 and 29.5 Ma, based on the revised age range of the fauna of quarries I and M of the Jebel Qatrani Formation of the Fayum depression by Seiffert, 2006); *Dolichocebus*, 20.5 Ma (mean of 21.0 and 20.0 Ma age provided by Kay, 2015); *Homunculus*, 17.2 Ma (mean of 17.9 and

306 16.5 Ma age provided by Kay, 2015); and *Oreopithecus* 6.75 Ma (mean of 7.0 and 6.5 Ma
307 for the last occurrence according to Rook et al., 2000).

308 The phylogenetic signal embedded in the shape data was measured using Pagel's
309 λ (Pagel, 1999) and Blomberg's K (Blomberg et al., 2003), together with the multivariate
310 version of Blomberg's K (K_{mult}; Adams, 2014). Pagel's λ and Blomberg's K were computed
311 using the 'phylosig' function of the 'phytools' package in R, while K_{mult} was computed with
312 the 'physignal' function of the 'geomorph' package v. 3.1.0 in R (Adams et al., 2019).
313 These metrics were computed based on extant taxa only (Arnold et al., 2010).

314 Ancestral node morphologies were computed from the bgPC scores for the last
315 common ancestors (LCAs) estimated by means of maximum likelihood, which were
316 rotated and translated from the morphospace back into the deformation field space,
317 generating a set of momentum vectors that were used in Deformetrica 4 to warp the
318 template surface into the target LCA morphology. Volumetric proportions for the LCAs
319 were computed based on the rescaled 3D models obtained from the phylomorphospace
320 approach; the scaling factor for each LCA was estimated using the 'anc.ML' function of the
321 R package 'phytools'. Morphological similarities between *Epipliopithecus* and the LCA
322 centroids were assessed by means Euclidean distances between the *Epipliopithecus*
323 centroid and the LCA bgPC scores, weighted on the basis of the percentage of variance
324 explained by each bgPC and computed using the 'distances' function of the 'distances'
325 package version 0.1.8 in R (Savje, 2019).

326 The two phylogenetic hypotheses for *Epipliopithecus* depicted in Figure 3 were
327 assessed further based on the coding of seven discrete characters that were deemed of
328 phylogenetic significance based on shape comparisons and analyses. The resulting
329 character-taxon matrix was analyzed for character congruence against a fixed topology
330 consistent with the phylogenetic hypotheses depicted in Figure 3. For both cladograms,
331 three indices customarily employed in cladistics (Farris, 1989) were computed in PAUP* v.

4.0a168 for Mac (Swofford, 2003) to assess the most parsimonious hypothesis: the consistency index (CI), the retention index (RI), and the rescaled consistency index (RC).

3. Results

3.1. Description and comparisons

The three bony labyrinths of *E. vindobonensis* are well preserved—except for the lateral canal of NMB OE 303b, which shows a small fracture in the bony encasing—and are not affected by diagenetic deformation, thereby permitting a straightforward extraction of the 3D surfaces of the vestibular apparatus bony labyrinth (Fig. 4a–c). Overall, the canals are fairly slender, as in platyrrhines and cercopithecins, falling within their variability as shown by a bivariate plot of SC volume vs. length (Fig. 5; Table 2; SOM Table S3). The bony vestibule is large, albeit less so than in hominids. The anterior and posterior canals are larger than the lateral canal, as in platyrrhines (Fig. 4e–i) and modern humans (Fig. 4u).

The *E. vindobonensis* common crus (CC) is long, as in extant platyrrhines (Fig. 4g–i) and in *Dolichocebus* (Fig. 4e), but unlike in most catarrhines. The trajectories of the anterior and posterior canal form a right angle when merging at the CC apex. Despite some similarities, the morphology of *Epipliopithecus* is clearly distinguishable from that of *Dolichocebus* and *Parapithecus* (Fig. 4d), as the CC is not posteromedially inclined and the anterior canal connection is placed more laterally.

The anterior canal of *E. vindobonensis* is slightly wider than tall (as in *Hoolock*; Fig. 4q), yet clearly rounded and lacking the vertical compression characteristic of extant hominoids (Fig. 4o–u), the anterosuperior elongation typical of hylobatids and *Pongo* (Fig. 4o–r; Urciuoli et al., 2020), and the extreme superior projection found in *Ateles* (Fig. 4g). The anterior canal of *Epipliopithecus* further differs from that of the stem anthropoid *Parapithecus* (Fig. 4d), the stem platyrrhine *Dolichocebus* (Fig. 4e), and the stem

358 catarrhine *Aegyptopithecus* (Fig. 4j), characterized by an almost triangular morphology
359 (albeit less so in the last genus). The superiormost portion of the anterior canal bends
360 medially, causing a moderate torsion of the canal trajectory. This morphology is also found
361 in the stem platyrrhine *Homunculus* (Fig. 4f) and, to a lesser extent, *Chlorocebus* (Fig. 4l)
362 and *Dolichocebus* (Fig. 4e), while in most cercopithecoids it is much more bent (e.g.,
363 *Macaca*; Fig. 4m). A sinuous trajectory of the anterior canal, although with a different
364 morphology, is also displayed by other taxa (e.g., *Cebus*; Fig. 4i) and thus is not very
365 informative from a phylogenetic viewpoint. Despite the aforementioned similarities,
366 *Epipliopithecus* differs from the stem platyrrhines *Homunculus* (Fig. 4f) and *Dolichocebus*
367 (Fig. 4e), from most extant platyrrhines (particularly *Ateles*; Fig. 4g), and from the stem
368 catarrhine *Aegyptopithecus* (Fig. 4j), in displaying a much less mediolaterally compressed
369 anterior canal.

370 The posterior canal of *Epipliopithecus* is slightly taller than wide, similar to that of
371 *Alouatta* (Fig. 4h) and *Symphalangus* (Fig. 4p), but differs from the latter by displaying a
372 less arched connection with the CC. The orientation of the posterior canal relative to the
373 plane defined by the anterior canal is different in the two individuals of *Epipliopithecus*: it
374 forms an obtuse angle in NHMW 1970/1397/0003 (resembling the hylobatid condition), but
375 forms a right angle in NMB OE 303 (as in other anthropoids; SOM Fig. S2).

376 The lateral canal is rounded and smaller than the other canals (more so in NMB OE
377 303), as in stem platyrrhines (Fig. 4e, f) and the stem catarrhine *Aegyptopithecus* (Fig. 4j),
378 although in *Epipliopithecus* this canal is not strongly compressed mediolaterally as in the
379 latter taxon (Fig. 4j). The trajectory of the ampullary portion of the lateral canal slightly
380 bends superiorly (more so in NMB OE 303; Fig. 4b, c), while the insertion of its slender
381 part is located anteriorly to the base of the CC (particularly in NHMW 1970/1397/0003; Fig.
382 4a), so that—as in extant hominoids but unlike cercopithecoids—the lateral canal does not
383 intersect the plane defined by the posterior canal. The lateral canal also shows a wave-like

shape, with its lateral-most tip pointing downwards, superficially resembling some individuals of *Pongo* (Fig. 4r), while differing from the morphology of *Trachypithecus* (Fig. 4k) and *Macaca* (Fig. 4m), where the canal bends inferiorly right before the ampullary portion.

3.2. Shape analysis

The bgPCA discriminates major anthropoid clades with just minimal overlap when the three axes are considered simultaneously (Fig. 6), thus closely resembling the previous results by Urciuoli et al. (2020) despite the increased number of platyrrhine taxa included here. The bgPCA results reported in Figure 6 closely resemble those derived using a cross-validated bgPCA (SOM Fig. S1), indicating that group separation is not spurious (Cardini and Polly, 2020).

The first principal component (bgPC1, which explains 59% of the variance) mainly reflects differences in volumetric proportions among the SCs and the volume they occupy relative to that of the bony vestibule, separating hominids (stout canals; quite negative scores) from both cercopithecoids and hylobatids (slender canals; positive to slightly negative scores), while platyrrhines (including stem taxa), the stem anthropoid *Parapithecus*, the stem catarrhine *Aegyptopithecus*, the stem hominoid *Oreopithecus*, and *Epipliopithecus* occupy an intermediate position in the morphospace. In particular, the two *Epipliopithecus* individuals, due to their fairly slender canals (Fig.4a–c), display similar intermediate scores along this axis, overlapping extensively with both extant and extinct platyrrhines in the overlap zone of cercopithecoids and hominoids (Fig. 6a, c).

In turn, bgPC2 (which explains 30% of the variance) accounts for differences in the size and shape of the anterior and posterior canals (Fig. 6a, d), in the position of the lateral canal ampullary insertion on the vestibule, and in CC length, separating most platyrrhines (positive scores) from catarrhines (moderately positive to negative scores). In particular,

platyrrhines possess large and very superiorly elongated canals in the portion close to the CC apex, as well as a flat lateral canal, which also connects more inferiorly on the vestibule with its ampullary portion. Catarrhines are more variable in these features, showing rounded to vertically compressed anterior and posterior canals, a shorter CC, and a variably sinuous lateral canal with its ampullary portion connecting more superiorly. *Epipliopithecus* displays moderately positive scores, falling within the range of several extant platyrrhines (*Aotus*, *Alouatta*, *Callithrix* and *Callicebus*), due to their large anterior and posterior canals, coupled with a long CC and a small lateral canal. Both the stem platyrrhines and *Oreopithecus* show similar moderately positive scores, while *Aegyptopithecus* and *Parapithecus* show markedly positive values due to their superiorly elongated vertical canals (Fig. 6a).

Finally, bgPC3 (which explains 11% of the variance) is driven by the position of the lateral canal relative to the posterior one, by the size and orientation of the posterior canal, as well as the shape of the anterior canal and CC thickness (Fig. 6b, e), separating hylobatids (most positive values) from most extant and fossil anthropoids (intermediate to negative scores). Hylobatids have a much larger gap between the lateral and posterior canals than other anthropoids except some modern humans, and their posterior canal is also smaller than, and forms an obtuse angle with, the large and anteriorly-protruding anterior canal. In contrast, in most cercopithecoids, *Aotus*, and *Callithrix,* the lateral canal broadly intersects with the posterior canal, while in the African great apes, *Theropithecus*, and *Cebus* the canals are only minimally separated. In addition, in all extant anthropoids except hylobatids, the plane of the posterior canal forms a right angle with the anterior canal, which does not project anteriorly. Both *Epipliopithecus* individuals display positive scores (NMB OE 303 with lower values), overlapping with some hylobatids (mainly *Hoolock*) and other extant anthropoids (particularly the hominids *Homo* and *Pongo*, the platyrrhines *Ateles* and *Alouatta*, and the cercopithecoids *Theropithecus* and *Piliocolobus*).

436 The slightly dissimilar bgPC3 scores for the two *Epipliopithecus* individuals result from
437 differences in orientation between the posterior and anterior canals (obtuse angle in
438 NHMW 1970/1397/0003 vs. right angle in NMB OE 303; SOM Fig. S2), causing a wider
439 separation between the lateral and posterior canals (Fig. 4a–c).
440 When the three bgPCs are considered together, the two *Epipliopithecus* individuals
441 show the greatest morphological similarities with platyrrhines (less so in NHMW
442 1970/1397/0003), as demonstrated by Mahalanobis distances from group centroids and by
443 their posterior probabilities of group membership (Table 3), leading us to reject close
444 similarities to the remaining groups for NMB OE 303, and to all anthropoid groups for
445 NHMW 1970/1397/0003 ($p < 0.05$). *Aegyptopithecus*, *Parapithecus*, *Oreopithecus*, and
446 stem platyrrhines also closely resemble extant New World monkeys, with *Oreopithecus*
447 also showing marginal affinities with cercopithecoids (Table 3). We obtain very similar
448 results when considering all catarrhines as a single group, with all fossils being classified
449 as platyrrhines (Table 4). For *Oreopithecus* and NHMW 1970/1397/0003, group
450 membership for catarrhines cannot be rejected. However, both specimens show much
451 lower Mahalanobis distances to the platyrrhine centroid (almost three times) than to that of
452 catarrhines. The two *Epipliopithecus* individuals are closer to one another than they are to
453 other fossil taxa (except for one individual of *Homunculus*, MPM-PV 3501), in turn showing
454 similarities with stem platyrrhines, *Aegyptopithecus* and *Oreopithecus* (Table 5). A cluster
455 analysis based on the momenta of the deformation fields confirms these results (Fig. 7).
456 *Epipliopithecus* clusters with *Alouatta* and *Ateles* (large and rounded vertical canals and a
457 large gap between the lateral and posterior canals), as well as *Pithecia* (obtuse angle
458 formed by the anterior and posterior canals), within a larger cluster that includes the
459 remaining extant platyrrhines and the other fossil taxa included in the analysis. In
460 particular, *Aegyptopithecus* and *Homunculus* cluster with *Saimiri* and *Cebus* (flat lateral
461 canal and similarities in the anterior canal morphology), while *Oreopithecus* clusters with

462 *Callicebus* (orientation of the anterior and posterior canals). Hylobatids cluster within a
463 larger group that also includes most cercopithecoids, and extant great apes cluster
464 together due to their distinctive stout volumetric proportions (Urciuoli et al., 2020).
465
466 *3.3. Phylogenetic signal and phylomorphospace*
467 Like previous analyses (Urciuoli et al., 2020; del Rio et al., 2020; Morimoto, et al.,
468 2020, our results indicate that the vestibule and SCs embed significant phylogenetic signal
469 (K_{mult} = 1.134, p < 0.001), suggesting these traits conform to a Brownian motion model of
470 evolution, with closely related taxa resembling one another slightly more than expected
471 (K_{mult} > 1). The phylogenetic signal computed for each bgPC separately is significant in all
472 instances (Table 6), with bgPC1 and bgPC2 suggesting the same evolutionary mode as
473 K_{mult} (K > 1). Conversely, we observe that the variance accumulates within clades for
474 bgPC3 (K < 1), thus suggesting that changes along this axis might be more strongly
475 affected by homoplasy.
476 The phylogenetic signal detected justifies the application of the phylomorphospace
477 approach (Fig. 8). The results indicate that the reconstructed LCAs of crown anthropoids
478 (Fig. 9a) and crown catarrhines (Fig. 9c) fall within the variability of extant New World
479 monkeys, being very close to the platyrrhine LCA (Fig. 9b)—irrespective of the
480 phylogenetic hypothesis used in the analysis for *Epipliopithecus* (i.e., stem catarrhine vs.
481 stem hominoid, Figs. 3 and 8; SOM Fig. S3). Cercopithecoids and hominoids appear much
482 more derived in SC morphology than platyrrhines, but in different directions. The crown
483 anthropoid, crown platyrrhine and crown catarrhine LCAs are reconstructed as possessing
484 large and slightly vertically-elongated canals (more so in the crown anthropoid and crown
485 platyrrhine LCAs; Fig. 9a, b) coupled with a long CC (shorter in the crown catarrhine LCA;
486 Fig. 9c), intermediate volumetric proportions (similar to those found in New World monkeys
487 and cercopithecins; Fig. 10), and a coplanar lateral canal that does not intersect the plane

of the posterior one (Fig. 9a–c). The LCA of crown catarrhines also shows a slightly more superiorly bent ampullary portion, more so than in *Epipliopithecus* (Fig. 9c). In contrast, the reconstructed crown hominoid LCA (Fig. 9d) is found in an area of the morphospace devoid of extant taxa and, according to our estimation, it already displayed some derived characters that are not found in *Epipliopithecus* (i.e., moderately vertically-compressed anterior canal, stouter canal proportions, lateral ampulla connecting more superiorly with the vestibule).

From a phenetic viewpoint, based on weighted Euclidean distances between *Epipliopithecus* and the bgPC scores for the reconstructed LCAs (Table 7), the former taxon is most similar to the crown catarrhine ancestral condition, and also closer to the crown anthropoid and platyrrhine LCAs, than to the ancestral conditions reconstructed for either hominoids or cercopithecoids.

We further synthesized the information provided by the phylomorphospace approach by defining seven discrete characters coded in a cladistic fashion (Table 8; Fig. 11). Their coding for the reconstructed LCAs as well as both extant and extinct anthropoids included in the analyses is reported in Table 9 and SOM Table S4. When the character states for extinct and extant taxa are analyzed against the two phylogenetic hypotheses by considering parsimony as a criterion (Table 10), *Epipliopithecus* is more parsimoniously interpreted as a stem catarrhine (Fig. 3a) than as a stem hominoid (Fig. 3b). The phylogenetic implications of the seven coded characters (Fig. 11; Tables 8 and 9; SOM Table S4) are discussed below and illustrated in Figure 12.

Size of the vestibule relative to the semicircular canals Extant hominids differ from all the remaining extant taxa in possessing a relatively larger vestibule, which may be thus interpreted as a synapomorphy of at least crown hominids. Among the extinct taxa, only the purported stem hominoid *Oreopithecus* displays the derived hominid condition, indicating either an independent acquisition of this feature in this taxon (as supported by

514 our LCA reconstructions) or a secondary reversal in hylobatids. *Epipliopithecus*, in any
515 case, retains the plesiomorphic condition of nonhominoid anthropoids.
516 Robusticity of the semicircular canals This character has the same distribution as the size
517 of the vestibule relative to the SCs. Extant hominids and *Oreopithecus* differ from the
518 remaining taxa by displaying stouter proportions. Accordingly, such proportions might be
519 interpreted either as convergent between *Oreopithecus* and hominids, or as a hominoid
520 synapomorphy with subsequent reversal in hylobatids. Our LCA reconstructions do not
521 provide clear support for either possibility, as they suggest an intermediate ancestral
522 condition in the overlap zone between hominoids and nonhominoid catarrhines. In either
523 case, for this character *Epipliopithecus* displays the more plesiomorphic condition of
524 nonhominoid anthropoids.
525 Shape of the anterior semicircular canal This character is more variable than the
526 preceding ones, both within anthropoid subclades, and sometimes even within the same
527 species. However, extant catarrhines generally differ from platyrrhines by possessing an
528 anterior canal that is not superiorly elongated, being instead either rounded (as in humans
529 and most cercopithecoids) or vertically compressed (as in great apes and generally
530 hylobatids, although in the latter it varies intraspecifically between rounded and vertically
531 compressed). Our LCA reconstructions suggest that the ancestral anthropoid condition—a
532 superiorly elongated anterior canal—is symplesiomorphic not only for platyrrhines but also
533 for the stem catarrhine *Aegyptopithecus*. They further support the view that a rounded
534 anterior SC is synapomorphic of crown catarrhines, while a vertically compressed anterior
535 SC would be synapomorphic for crown hominoids + *Oreopithecus*. In this regard,
536 *Epipliopithecus* is more derived than *Aegyptopithecus* but less so than *Oreopithecus*. This
537 character, therefore, unambiguously supports for *Epipliopithecus* a catarrhine status more
538 derived than in *Aegyptopithecus*, although it would be consistent with either a stem
539 catarrhine or a stem hominoid status.

Shape of the anterior portion of the semicircular canal Hylobatids and orangutans differ from the rest of the sample by displaying an anterosuperiorly-projecting anterior portion of the anterior canal. This condition may be interpreted as a crown hominoid synapomorphy subsequently reversed in hominines, as further supported by the fact that *Oreopithecus* displays the derived condition for hominoids. Alternatively, this feature might have been independently acquired in *Oreopithecus*, as suggested by our LCA reconstructions, which only recover it as a hylobatid synapomorphy. Given the possession of other SC hominoid synapomorphies in *Oreopithecus*, we tend to favor the former interpretation, even if both are equally parsimonious. In any case, *Epipliopithecus* retains the more plesiomorphic condition of non-hominoid anthropoids.

Shape of the posterior semicircular canal Although this character is somewhat variable within anthropoid subclades and sometimes even within species, some generalities can be drawn. In platyrrhines, the posterior canal is generally elongated superiorly to some extent, whereas most cercopithecoids have a rounded posterior canal, and hominoids generally vary between a rounded and a vertically compressed morphology (only sometimes superiorly elongated in *Pan*). Our LCA reconstructions indicate that platyrrhines and *Aegyptopithecus* retain the ancestral anthropoid condition (superiorly elongated posterior canal), whereas the rounded morphology would be synapomorphic for crown hominoids. *Epipliopithecus* displays the plesiomorphic anthropoid condition and thus differs from *Oreopithecus*, which displays the derived catarrhine morphology.

Shape of the lateral semicircular canal ampullary portion Extant hominoids differ from the remaining extant taxa and all the analyzed extinct genera by displaying a markedly superiorly-bent ampullary portion of the lateral canal. Both *Epipliopithecus* and *Oreopithecus* thus display a more plesiomorphic condition than crown hominoids, as further confirmed by our LCA reconstructions.

Length of the common crus This character is also variable to some extent, but platyrrhines generally display a longer CC than extant catarrhines, with hominoids having an even shorter CC than most cercopithecoids. Our LCA reconstructions support an intermediate length of the CC as synapomorphic of crown catarrhines, with a short CC being synapomorphic for hominoids. *Epipliopithecus* resembles *Aegyptopithecus* and platyrrhines by retaining the ancestral anthropoid condition, whereas *Oreopithecus* displays the derived hominoid morphology.

4. Discussion

Our analysis of the SC and vestibule morphology of *Epipliopithecus* allows us to refine our understanding of the evolution of this anatomical region in anthropoid primates and to refine previous hypotheses proposed by Urciuoli et al. (2020). The results of our deformation-based 3DGM analysis and the reconstruction of ancestral morphotypes for main anthropoid clades indicate that, like the stem catarrhine *Aegyptopithecus*, *Epipliopithecus* displays a platyrrhine-like morphology most similar to that reconstructed for the crown catarrhine LCA. This might be compatible with *Epipliopithecus* being either a stem catarrhine, or a crown catarrhine only slightly postdating the cercopithecoid-hominoid split. However, the fact that *Epipliopithecus* most closely resembles the crown anthropoid (and platyrrhine) LCAs (Table 7) suggests that the semicircular morphology of this taxon is most consistent with its status as a stem catarrhine. This conclusion is further supported by the analysis of seven discrete characters coded for this anatomical area—which indicate that this is the most parsimonious hypothesis, for reasons discussed in greater detail below.

4.1. Epipliopithecus *as a hominoid*

590 Based on the morphology of the SCs and vestibule, *Epipliopithecus* lacks multiple
591 hominoid synapomorphies, including a large vestibule relative to the canals, stout SCs,
592 vertically-compressed anterior canal, anterosuperiorly- projecting anterior portion of the
593 anterior canal, markedly superiorly-bent ampullary portion of the lateral canal, and short
594 CC. Urciuoli et al.(2020) already interpreted some of these features (vertically-compressed
595 anterior canal and markedly superiorly-bent ampullary portion of the lateral canal) as
596 potential crown hominoid synapomorphies, whereas they interpreted others (large
597 vestibule and stout canals) as hominid synapomorphies. Urciuoli et al. (2020) interpreted a
598 superiorly-bent ampullary portion of the lateral canal as a hominoid synapomorphy.
599 However, hominoids are, in fact, characterized by the possession of a markedly bent
600 trajectory, whereas other catarrhines display a flat to slightly superiorly-bent ampullary
601 portion of the lateral canal. This is the case for *Epipliopithecus*, which displays much less
602 bending of the lateral canal than in *Oreopithecus* or any extant hominoid.
603 The possession of a large vestibule and stout canals was previously interpreted as
604 being synapomorphic for hominids (Urciuoli et al., 2020) because hylobatids display a
605 different ('monkey-like') condition. The differences in volumetric proportions between
606 *Epipliopithecus* and hominids are particularly clear (Fig. 10), with the former closely
607 resembling platyrrhines, *Aegyptopithecus*, and the inferred ancestral catarrhine condition.
608 Given that both features are present in *Oreopithecus*, they may be interpreted as hominoid
609 synapomorphies subsequently reversed in hylobatids—thereby supporting a more basal
610 branching for *Epipliopithecus*. However, their interpretation as hominid synapomorphies is
611 equally parsimonious, as it would only imply their independent acquisition in *Oreopithecus*.
612 Therefore, neither a large vestibule nor stout canals can be used to unambiguously
613 discount a hominoid status for *Epipliopithecus*. A similar caveat applies to the lack of an
614 anterosuperiorly-projecting anterior canal in *Epipliopithecus*. This condition was previously
615 interpreted as an autapomorphy of *Hylobates* (Le Maître, et al., 2017) or as a hylobatid

synapomorphy (Spoor and Zonneveld, 1998; Urciuoli, et al. 2020). However, given its presence in orangutans and *Oreopithecus*, it is more readily interpreted as a hominoid synapomorphy subsequently reversed in hominines. The interpretation of some of the potential hominoid synapomorphies lacking in *Epipliopithecus* is ambiguous due to homoplasy (convergence and/or reversal). However, it is worth noting that, except for the markedly superiorly bent ampullary portion of the lateral canal, *Oreopithecus* further displays two more unambiguous hominoid synapomorphies (vertically compressed anterior canal and short CC). The absence of these features in *Epipliopithecus* thus conclusively excludes a more derived hominoid status for the latter as compared with *Oreopithecus*.

Epipliopithecus also displays some hylobatid-like features in the spatial configuration between the lateral and posterior canals, as well as in the orientation between the anterior and posterior canals. According to Urciuoli et al. (2020), the lack of intersection between the lateral and posterior canals and the presence of an obtuse angle between the anterior and posterior canals would be synapomorphic for hominoids and hylobatids, respectively. However, only *Hylobates* consistently displays both features, while most anthropoid taxa, as well as the two *Epipliopithecus* individuals, show a considerable amount of intraspecific variation. Hence, we refrained from coding these features in a cladistic manner, especially in view of the low phylogenetic signal ($K < 1$) recovered for bgPC3 (accounting for the variation in the configuration of these features), which suggests a substantial degree of homoplasy. Indeed, previous analyses hypothesized that suspensory species possess more obtuse angles between the vertical canals (Gonzales et al., 2019), as this configuration provides an increased sensitivity for pitch (at the expense of roll) head movements (Muller and Verhagen, 2002a,b,c). The similarities between NHMW 1970/1397/0003, hylobatids, and some atelids (Spoor and Zonneveld, 1998; Gonzales et al., 2019) would thus agree with previous inferences about the locomotor repertoire of this taxon including some degree of suspensory behaviors

642 (Zapfe, 1958; Fleagle, 1983; Langdon, 1986; Rose, 1994; Arias Martorell et al., 2015). In
643 contrast, the more plesiomorphic condition of NBM OE 303III (characterized by tangent
644 lateral and posterior canals, and vertical canals approximating a right angle), also found in
645 *Aegyptopithecus* and some nonsuspensory platyrrhine species, suggests caution when
646 using SC orientation alone for inferring positional behaviors (Perier et al., 2016; contra
647 Malinzak et al., 2012; Berlin et al., 2013).
648
649 *4.2.* Epipliopithecus *as a stem catarrhine*
650 *Epipliopithecus* resembles both stem platyrrhines and the stem catarrhine
651 *Aegyptopithecus* in lacking all of the aforementioned hominoid synapomorphies, thereby
652 retaining the plesiomorphic anthropoid condition—a relatively small vestibule, slender SCs,
653 anterosuperiorly nonprojecting anterior portion of the anterior canal, superiorly elongated
654 posterior canal, ampullary portion of the lateral canal not markedly bent superiorly, and
655 long CC. The fact that *Epipliopithecus* lacks hominoid synapomorphies displayed by
656 *Oreopithecus* could still be consistent with a more basal stem hominoid status. However,
657 such an interpretation is contradicted by the retention in *Epipliopithecus* of a superiorly
658 elongated posterior canal and a long CC—contrasting with the rounded posterior canal
659 and moderately short CC that are synapomorphic of crown catarrhines. The catarrhine
660 status of *Epipliopithecus* and other pliopithecoids is well established based on multiple
661 features, such as the loss of the second premolars and the presence of a C^1/P_3 honing
662 complex (e.g., Harrison, 2013). The catarrhine status of *Epipliopithecus* is further
663 supported by the possession of a rounded anterior canal, which is intermediate between
664 the primitive morphology (superiorly elongated anterior canal) retained by platyrrhines and
665 *Aegyptopithecus*, and the more derived (vertically compressed) morphology
666 synapomorphic of hominoids. In this regard, *Epipliopithecus* is more derived toward crown
667 catarrhines than the propliopipithecoid *Aegyptopithecus*, in agreement with other cranial

features such as the possession of a partially enclosed tubular ectotympanic in *Epipliopithecus* (e.g., Harrison, 2013).

In summary, based on the morphology of the SCs and vestibule, *Epipliopithecus* is most parsimoniously interpreted as a stem catarrhine more derived than *Aegyptopithecus*, due to its possession of a crown catarrhine synapomorphy—rounded anterior canal—coupled with the lack of two additional crown catarrhine synapomorphies (superiorly elongated posterior canal and long CC) and multiple hominoid and/or hominid synapomorphies as described above. The shapes of the anterior and posterior canals and CC should be considered with caution in light of the intraspecific variability displayed by these characters in some taxa (SOM Table S4). Previous analyses noted a structural relationship between the morphology of these canals and the extension of the subarcuate fossa (Jeffery and Spoor, 2006; Jeffery et al., 2008), and this relationship has been uncritically assumed in some studies (Spoor et al., 2007; Silcox et al., 2009; Gonzales et al., 2019). However, in most cases the fossa simply expands within the space left available from the ossification of the canals, with little or no influence on their shape (Jeffery et al., 2008; see also Urciuoli et al., 2020). In support of the latter hypothesis, we observe meager dissimilarities in the anterior canal morphology of NHMW 1970/1397/0003 and NBM OE 303III—except for the angle, as discussed above—irrespective of the marked differences in the morphology of the fossa between the two individuals (Zapfe, 1960). While a large amount of morphological variation has been documented within ruminant genera (Mennecart and Costeur, 2016), variation in CC length and shape has not been exhaustively analyzed in primates (Spoor and Zonneveld, 1998; Ekdale 2013; Lee et al., 2013). In the present study, we found considerable intraspecific variation in CC length for some species of monkeys and apes. Nevertheless, our results support a clear morphocline from the ancestral condition (long CC) retained by platyrrhines, *Aegyptopithecus*, and *Epipliopithecus*, to the most derived condition (short CC) characteristic of hominoids, with

694 cercopithecoids displaying an intermediate condition that is likely synapomorphic for crown
695 catarrhines as a whole. Therefore, *Epipliopithecus* SC morphology supports its
696 interpretation as more derived than *Aegyptopithecus* toward crown catarrhines, but
697 excludes a crown catarrhine status and, in particular, a closer relationship with hominoids
698 (unlike in the case of *Oreopithecus*).
699
700 **5. Conclusions**
701 Our results are in broad agreement with previous analyses suggesting that
702 *Epipliopithecus* displays a 'typical monkey' inner ear morphology (Morimoto et al., 2020),
703 while *Oreopithecus* possesses SC and vestibule features derived toward the crown
704 hominoid condition (Urciuoli et al., 2020). At the same time, our study further refines
705 previous comparisons of SC and vestibule morphology between *Epipliopithecus* and other
706 anthropoids, enabling us to test competing hypotheses about the phylogenetic position of
707 this taxon (i.e., stem catarrhine vs. stem hominoid).
708 From a phenetic viewpoint, for this anatomical area *Epipliopithecus* more closely
709 resembles platyrrhines and the stem catarrhine *Aegyptopithecus*, as well as the
710 reconstructed ancestral catarrhine morphotype. The fact that *Epipliopithecus* shows
711 greater similarities with the platyrrhine and anthropoid ancestral morphotypes, rather than
712 with those of cercopithecoids or hominoids, supports the view that *Epipliopithecus* is a
713 stem catarrhine instead of a stem hominoid. From a cladistic perspective, this
714 interpretation is confirmed based on a series of crown catarrhine and crown hominoid
715 synapomorphies. *Epipliopithecus* is more parsimoniously interpreted as a stem catarrhine
716 than as a stem hominoid based on the vestibular morphology analyzed here because it
717 lacks several catarrhine and all hominoid synapomorphies. Specifically, the possession of
718 a rounded posterior canal reinforces the view that *Epipliopithecus* is more derived than
719 *Aegyptopithecus* among stem catarrhines.

The information provided by the SCs and vestibule is thus congruent with the ectotympanic morphology of *Epipliopithecus* (see review in Fricano, 2018), which is more plesiomorphic than in crown catarrhines but more derived than in propliopithecoids. Some similarities between *Epipliopithecus* and hylobatids are based on characters that are too variable within species to be of use for phylogenetic assessment. Such features might have evolved independently between some atelids and hylobatids, due to similar locomotor-related selection pressures, and do not support the close phylogenetic link classically hypothesized between pliopithecoids and hylobatids (Hürzeler, 1954; Zapfe, 1960, 1961; Simons and Fleagle, 1973), particularly given that *Epipliopithecus* displays no crown hominoid synapomorphies. We therefore conclude that the SC and vestibular morphology reinforces the most commonly held view that, in accordance with most (Zalmout et al., 2010; Stevens et al., 2013; Nengo et al., 2017) but not all (Alba et al., 2015) recent cladistic analyses, *Epipliopithecus* is best interpreted as a stem catarrhine rather than a stem hominoid.

Acknowledgements

This research has been funded by the Agencia Estatal de Investigación (CGL2016-76431-P and CGL2017-82654-P, AEI/FEDER EU; and BES-2015-071318 to A.U.), the Generalitat de Catalunya (CERCA Programme, and consolidated research groups 2017 SGR 86 and 2017 SGR 116 GRC), the French Centre National de la Recherche Scientifique, the Leakey Foundation (research grant), and the Synthesys Project (AT-TAF-4689; http://synthesys3.myspecies.info/), which is financed by the European Community Research Infrastructure Action under the FP7. Part of the analyses were performed using High Performance Computing resources from BSC (BCV-2020-1-0008). We are grateful to Jose Torres for the technical help provided in the setup of the analysis. We thank the following people for providing or permitting access to CT scans: Ursula Göhlich

(*Epipliopithecus* NHMW 1970/1397/0003), Martin Dockner, Loïc Costeur (*Epipliopithecus* NMBOE 303), Lorenzo Rook (*Oreopithecus*), José Braga (human specimens), Lynn Copes, Lynn Lucas, and the MCZ (part of the scans used in the study, funded by NSF DDIG #0925793 and Wenner-Gren Foundation Dissertation Grant #8102 to Lynn Copes), Richard Kay (*Homunculus* and *Dolichocebus*),Timothy Ryan (*Aegyptopithecus*; funded by NSF BCS-0416164 to Timothy Ryan and the Leakey Foundation), and the Division of Fossil Primates of the Duke Lemur Center (*Parapithecus*). We also thank Erik Seiffert and Steven Heritage for providing a digital rendering of *Parapithecus*. Finally, we thank the Editor (Andrea Taylor), the Associate Editor, and three anonymous reviewers for useful comments that helped us to improve a previous version of this paper.

References

Adams, D.C., 2014. A generalized K statistic for estimating phylogenetic signal from shape and other high-dimensional multivariate data. Syst. Biol. 63, 685–697.

Adams D.C, Collyer, M.L., Kaliontzopoulou, A., 2019. Geomorph: Software for geometric morphometric analyses. R Package Version. https://cran.rproject.org/package=geomorph.

Alba, D.M., Berning, B., 2013. On the holotype and original description of the pliopithecid *Plesiopliopithecus lockeri* (Zapfe, 1960). J. Hum. Evol. 65, 338–340.

Alba, D.M., Moyà-Solà, S., 2012. A new pliopithecid genus (Primates: Pliopithecoidea) from Castell de Barberà (Vallès-Penedès Basin, Catalonia, Spain). Am. J. Phys. Anthropol. 147, 88–112.

Alba, D.M., Moyà-Solà, S., Malgosa, A., Casanovas-Vilar, I., Robles, J.M., Almécija, S., Galindo, J., Rotgers, C., Bertó Mengual, J.V., 2010. A new species of *Pliopithecus* Gervais, 1849 (Primates: Pliopithecidae) from the Middle Miocene (MN8) of Abocador

771 de Can Mata (els Hostalets de Pierola, Catalonia, Spain). Am. J. Phys. Anthropol. 141,
772 52–75.
773 Alba, D.M., Almécija, S., DeMiguel, D., Fortuny, J., Pérez de los Ríos, M., Pina, M.,
774 Robles, J. M., Moyà-Solà, S., 2015. Miocene small-bodied ape from Eurasia sheds
775 light on hominoid evolution. Science 350, aab2625.
776 Almécija, S., Tallman, L., Sallam, H.M., Fleagle, J.G., Hammond, A.S., Seiffert, E.R.,
777 2019. Early anthropoid femora reveal divergent adaptive trajectories in catarrhine hind-
778 limb evolution. Nat. Commun. 10, 4778.
779 Andrews, P.J., Harrison, T., Delson, E., Bernor, R.L., Martin, L., 1996. Distribution and
780 biochronology of European and Southwest Asian Miocene catarrhines. In: Bernor,
781 R.L., Fahlbusch, V., Mittmann, H. (Eds.), The Evolution of Western Eurasian Neogene
782 Mammalian Faunas. Columbia University Press, New York, pp. 168–207.
783 Ankel, F., 1965. Der Canalis Sacralis als Indikator für die Länge der Caudalregion der
784 Primaten. Folia Primatol. 3, 263–276.
785 Arias-Martorell, J., Alba, D.M., Potau, J. M., Bello-Hellegouarch, G., Pérez-Pérez, A.,
786 2015. Morphological affinities of the proximal humerus of *Epipliopithecus*
787 *vindobonensis* and *Pliopithecus antiquus*: Suspensory inferences based on a 3D
788 geometric morphometrics approach. J. Hum. Evol. 80, 83–95.
789 Arnold, C., Matthews, L.J., Nunn, C.L., 2010. The 10kTrees website: A new online
790 resource for primate phylogeny. Evol. Anthropol. 19, 114–118.
791 Beaudet, A., Dumoncel, J., Thackeray, J.F., Bruxelles, L., Duployer, B., Tenailleau, C.,
792 Bam, L., Hoffman, J., de Beer, F., Braga, J., 2016. Upper third molar internal structural
793 organization and semicircular canal morphology in Plio-Pleistocene South African
794 cercopithecoids. J. Hum. Evol. 95, 104–120.
795 Begun, D.R., 2002 The Pliopithecoidea. In: Hartwig, W.C. (Ed.), 2002. The Primate Fossil
796 Record. Cambridge University Press, Cambridge, pp. 221–240.

797 Begun, D.R., 2017. Evolution of the Pliopithecoidea. In A. Fuentes (Ed.), *The International*
798 *Encyclopedia of Primatology* (pp. [1-4]): John Wiley & Sons.
799 Berlin, J.C., Kirk, E.C., Rowe, T.B., 2013. Functional implications of ubiquitous
800 semicircular canal non-orthogonality in mammals. PLoS One 8, e79585.
801 Billet, G., Hautier, L., Lebrun, R., 2015. Morphological diversity of the bony labyrinth (inner
802 ear) in extant xenarthrans and its relation to phylogeny. J. Mammal. 96, 658–672.
803 Blomberg, S.P., Garland, T., Ives, A.R., 2003. Testing for phylogenetic signal in
804 comparative data: behavioral traits are more labile. Evolution 57, 717–745.
805 Bône, A., Louis, M., Martin, B., Durrleman, S., 2018. Deformetrica 4: an open-source
806 software for statistical shape analysis. In: Reuter, M., Wachinger, C., Lombaert, H.,
807 Paniagua, B., Lüthi, M., Egger, B. (Eds.), Shape in Medical Imaging. Shape MI 2018.
808 Springer, Cham, pp. 3–13.
809 Bookstein, F.L., 2019. Pathologies of between-groups principal components analysis in
810 geometric morphometrics. Evol. Biol. 46, 271–302.
811 Braga, J., Samir, C., Risser, L., Dumoncel, J., Descouens, D., Thackeray, J.F., Barlesque,
812 P., Oettlé, A., Loubes, J.-M., Fradi, A., 2019a. Cochlear shape reveals that the human
813 organ of hearing is sex-typed from birth. Sci. Rep. 9, 10889.
814 Bush, E.C., Simons, E.L., Dubowitz, D.J., Allman, J.M., 2004. Endocranial volume and
815 optic foramen size in *Parapithecus grangeri*. In: Ross, C.F., Kay, R.F. (Eds),
816 Anthropoid Origins: New Visions. Kluwer/Plenum, New York, pp. 603–614.
817 Cardini, A., O'Higgins, P., Rohlf, F.J., 2019. Seeing distinct groups where there are none:
818 Spurious patterns from between-group PCA. Evol. Biol. 46, 303–316.
819 Cardini, A., Polly, P.D., 2020. Cross-validated between-group PCA scatterplots: A solution
820 to spurious group separation? Evol. Biol. 47, 85–95.

821 Casanovas-Vilar, I., Alba, D.M., Garcés, M., Robles, J.M., Moyà-Solà, S., 2011. Updated
822 chronology for the Miocene hominoid radiation in Western Eurasia. Proc. Natl. Acad.
823 Sci. USA 108, 5554–5559.
824 Ciochon, R.L., Corruccini, R.S., 1977. The phenetic position of *Pliopithecus* and its
825 phylogenetic relationship to the Hominoidea. Syst. Zool. 26, 290–299.
826 Coleman, M.N., Colbert, M.W. 2010. Correlations between auditory structures and hearing
827 sensitivity in non-human primates. J. Morphol. 271, 511–532.
828 Costeur, L., Grohé, C., Aguirre-Fernández, G., Ekdale, E., Schulz, G., Müller, B.,
829 Mennecart, B., 2018. The bony labyrinth of toothed whales reflects both phylogeny
830 and habitat preferences. Sci. Rep. 8, 7841.
831 David, R., Droulez, J., Allain, R., Berthoz, A., Janvier, P., Bennequin, D., 2010. Motion
832 from the past. A new method to infer vestibular capacities of extinct species. C.R.
833 Palevol 9, 397–410.
834 David, R., Stoessel, A., Berthoz, A., Spoor, F., Bennequin, D., 2016. Assessing
835 morphology and function of the semicircular duct system: introducing new in-situ
836 visualization and software toolbox. Sci. Rep. 6, 32772.
837 del Rio, J., Aristide, L., dos Reis, S.F., dos Santos, T.M.P., Lopes, R.T., Perez, S.I., 2020.
838 Allometry, function and shape diversification in the inner ear of platyrrhine primates. J.
839 Mammal. Evol. https://doi.org/10.1007/s10914-019-09490-9.
840 Delson, E., Andrews, P.J., 1975. Evolution and interrelationships of the catarrhine
841 primates. In: Luckett, W.P., Szalay, F.S. (Eds.), Phylogeny of the Primates: A
842 Multidisciplinary Approach. Plenum Press, New York, pp. 405–446.
843 Dumoncel, J., Durrleman, S., Braga, J., Jessel, J.P., Subsol, G., 2014. Landmark-free 3D
844 method for comparison of fossil hominins and hominids based on endocranium and
845 EDJ shapes. Am. J. Phys. Anthropol. 153 (S58), 110.

Durrleman, S., Pennec, X., Trouvé, A., Ayache, N., Braga, J., 2012. Comparison of the endocranial ontogenies between chimpanzees and bonobos via temporal regression and spatiotemporal registration. J. Hum. Evol. 62, 74–88.

Durrleman, S., Prastawa, M., Korenberg, J.R., Joshi, S., Trouvé, A., Gerig, G., 2012. Topology preserving atlas construction from shape data without correspondence using sparse parameters. In: Ayache, N., Delingette, H., Golland, P., Mori, K. (Eds.), Medical Image Computing and Computer-Assisted Intervention – MICCAI 2012. Springer, Berlin, pp. 223–230.

Ekdale, E.G., 2013. Comparative anatomy of the bony labyrinth (inner ear) of placental mammals. PLoS One 8, e66624.

Farris, J.S., 1989. The retention index and the rescaled consistency index. Cladistics 5, 417–419.

Fleagle, J.G., 1983. Locomotor adaptations of Oligocene and Miocene hominoids and their phyletic implications. In: Ciochon, R.L., Corruccini, R.S. (Eds.), New Interpretations of Ape and Human Ancestry. Plenum Press, New York, pp. 301–324.

Fleagle, J.G., 1984. Are there any fossil gibbons? In: Preuschoft, H., Chivers, D.J., Brockelman, W.Y., Creel, N. (Eds.), The Lesser Apes: Evolutionary and Behavioral Biology. Edinburgh University Press, Edinburgh, pp. 431–447.

Fricano, E.E.I., 2018. The primate ectotympanic tube: correlates of structure, function, and development. Ph.D. Dissertation, Johns Hopkins University.

Fulwood, E.L., Boyer, D.M., Kay, R.F., 2016. Stem members of Platyrrhini are distinct from catarrhines in at least one derived cranial feature. J. Hum. Evol. 100, 16–24.

Gilbert, C.C., Ortiz, A., Pugh, K.D., Campisano, C.J., Patel, B.A., Singh, N.P., Fleage, J.G., Patnaik, R., 2020. New middle Miocene ape (Primates: Hylobatidae) from Ramnagar, India fills major gaps in the hominoid fossil record. Proc. R. Soc. B 287, 20201655.

872 Glaunès, J.A., Joshi, S., 2006. Template estimation form unlabeled point set data and
873 surfaces for Computational Anatomy. in: Pennec, X., Joshi, S. (Eds.), MICCAI 2006
874 Workshop Proceedings. MFCA'06 Workshop. Mathematical Foundations of
875 Computational Anatomy: Geometrical and Statistical Methods for Modelling Biological
876 Shape Variability. INRIA/MICCAI, Conpenhagen, pp. 29–39.
877 Gonzales, L.A., Malinzak, M.D., Kay, R.F., 2019. Intraspecific variation in semicircular
878 canal morphology—A missing element in adaptive scenarios? Am. J. Phys. Anthropol.
879 168, 10–24.
880 Grohé, C., Tseng, Z. J., Lebrun, R., Boistel, R., Flynn, J.J., 2015. Bony labyrinth shape
881 variation in extant Carnivora: a case study of Musteloidea. J. Anat. 228, 366–383.
882 Grohé, C., Lee, B., Flynn, J.J., 2018. Recent inner ear specialization for high-speed
883 hunting in cheetahs. Sci. Rep. 8, 1–8.
884 Harrison, T., 1982. Small-bodied apes from the Miocene of East Africa. Ph.D. Dissertation,
885 University College London.
886 Harrison, T., 1987. The phylogenetic relationships of the early catarrhine primates: a
887 review of the current evidence. J. Hum. Evol. 16, 41–80.
888 Harrison, T., 2005. The zoogeographic and phylogenetic relationships of early catarrhine
889 primates in Asia. Anthropol. Sci. 113, 43–51.
890 Harrison, T., 2010. Dendropithecoidea, Proconsuloidea, and Hominoidea (Catarrhini,
891 Primates). In: Werdelin, L. (Ed.), Cenozoic Mammals of Africa. University of California
892 Press, Berkeley, pp. 429–469.
893 Harrison, T., 2013. Catarrhine origins. In: Begun, D.R. (Ed.), A Companion to
894 Paleoanthropology. Blackwell Publishing, Oxford, pp. 376–396.
895 Harrison, T., Gu, Y., 1999. Taxonomy and phylogenetic relationships of early Miocene
896 catarrhines from Sihong, China. J. Hum. Evol. 37, 225–277.

897 Harrison, T., Zhang, Y., Wei, G., Sun, C., Wang, Y., Liu, J., Tong, H., Huang, B., Xu, F.,
898 2020. A new genus of pliopithecoid from the late Early Miocene of China and its
899 implications for understanding the paleozoogeography of the Pliopithecoidea. J. Hum.
900 Evol. 145, 102838.
901 Harzhauser, M., Kroh, A., Mandic, O., Piller, W. E., Göhlich, U., Reuter, M., Berning, B.,
902 2007. Biogeographic responses to geodynamics: A key study all around the Oligo–
903 Miocene Tethyan Seaway. Zool. Anz. 246, 241–256.
904 Hürzeler, J., 1954. Contribution a l'odontologie et a la phylogénèse du genre *Pliopithecus*
905 Gervais. Ann. Paleontol. 40, 5–63.
906 Jeffery, N., Spoor, F., 2006. The primate subarcuate fossa and its relationship to the
907 semicircular canals part I: prenatal growth. J. Hum. Evol. 51, 537–549.
908 Jeffery, N., Ryan, T.M., Spoor, F., 2008. The primate subarcuate fossa and its relationship
909 to the semicircular canals part II: Adult interspecific variation. J. Hum. Evol. 55, 326–
910 339.
911 Kay, R.F., Simons, E., Ross, J.L., 2009a. The basicranial anatomy of African
912 Eocene/Oligocene anthropoids. Are there any clues for platyrrhine origins? In: Fleagle,
913 J.G., Gilbert, C.C. (Eds.), Elwyin Simons: A Search for Origins. Springer, New York,
914 pp. 125–158.
915 Kay, R.F., Fleagle, J.G., Mitchell, T.R.T., Colbert, M., Bown, T., Powers, D.W., 2009b. The
916 anatomy of *Dolichocebus gaimanensis*, a stem platyrrhine monkey from Argentina. J.
917 Hum. Evol. 54, 323–382.
918 Kay, R.F., 2015. Biogeography in deep time – What do phylogenetics, geology, and
919 paleoclimate tell us about early platyrrhine evolution? Mol. Phylogenet. Evol. 82, 358–
920 374.
921 Kirk, E.C., Gosselin-Ildari, A.D., 2009. Cochlear labyrinth volume and hearing abilities in
922 primates. Anat. Rec. 292, 765–776.

923 Kunimatsu, Y., Nakatsukasa, M., Shimizu, D., Nakano, Y., Ishida, H., 2019. Loss of the
924 subarcuate fossa and the phylogeny of *Nacholapithecus*. J. Hum. Evol. 131, 22–27.
925 Langdon, J.H., 1986. Functional morphology of the Miocene hominoid foot. Contrib.
926 Primatol. 22, 239e257.
927 Lebrun, R., P. de León, M., Tafforeau, P., Zollikofer, C., 2010. Deep evolutionary roots of
928 strepsirrhine primate labyrinthine morphology. J. Anat 216, 368–380.
929 Lebrun, R., Godinot, M., Couette, S., Tafforeau, P., Zollikofer, C., 2012. The labyrinthine
930 morphology of *Pronycticebus gaudryi* (Primates, Adapiformes). Palaeobiodiv.
931 Palaeoenvir. 92, 527–537.
932 Lee, J.Y., Shin, K.J., Kim, J.N., Yoo, J.Y., Song, W.C., Koh, K.S., 2013. A morphometric
933 study of the semicircular canals using micro-CT images in three-dimensional
934 reconstruction. Anat. Rec. 269, 834–839.
935 Le Maître A., Schuetz, P., Vignaud, P., Brunet, M.., 2017. New data about semicircular
936 canal morphology and locomotion in modern hominoids. J. Anat. 231, 95–109.
937 Macrini, T.E., Flynn, J.J., Ni, X., Croft, D.A., Wyss, A. R., 2013. Comparative study of
938 notoungulate (Placentalia, Mammalia) bony labyrinths and new phylogenetically
939 informative inner ear characters. J. Anat. 223, 442–461.
940 Malinzak, M.D., Kay, R.F., Hullar, T.E., 2012. Locomotor head movements and
941 semicircular canal morphology in primates. Proc. Natl. Acad. Sci. USA 109, 17914–
942 17919.
943 Manoussaki, D., Dimitriadis, E.K., Chadwick, R.S., 2006. Cochlea's graded curvature
944 effect on low frequency waves. Phys. Rev. Lett. 96, 088701.
945 Mennecart, B., Costeur, L., 2016. Shape variation and ontogeny of the ruminant bony
946 labyrinth, an example in Tragulidae. J. Anat. 229, 422–435.

947 Mennecart, B., Rössner, G. E., Métais, G., DeMiguel, D., Schulz, G., Müller, B., Costeur,
948 L., 2016. The petrosal bone and bony labyrinth of early to middle Miocene European
949 deer (Mammalia, Cervidae) reveal their phylogeny. J. Morphol. 277, 1329–1338.
950 Mennecart, B., DeMiguel, D., Bibi, F., Rössner, G.E., Métais, G., Neenan, J.M., Wang, S.,
951 Schulz, G, Müller, B., Costeur, L., 2017. Bony labyrinth morphology clarifies the origin
952 and evolution of deer. Sci. Rep. 7, 13176.
953 Mitteroecker, P., Bookstein, F., 2011. Linear discrimination, ordination, and the
954 visualization of selection gradients in modern morphometrics. Evol. Biol. 38, 100–114.
955 Moyà-Solà, S., Köhler, M., 2000. Comprendere *Oreopithecus bambolii*, un ominoide
956 fossile enigmatico. Atti Mus. St. Nat. Maremma 18, 39–65.
957 Moyà-Solà, S., Köhler, M., Alba, D.M., 2001. *Egarapithecus narcisoi*, a new genus of
958 Pliopithecidae (Primates, Catarrhini) from the late Miocene of Spain. Am. J. Phys.
959 Anthropol. 114, 312–324.
960 Morimoto, N., Kunimatsu, Y., Nakatsukasa, M., Ponce de León, M. S., Zollikofer, C. P.,
961 Ishida, H., Sasaki, T., Suwa, G., 2020. Variation of bony labyrinthine morphology in
962 Mio–Plio–Pleistocene and modern anthropoids. Am. J. Phys. Anthropol. 173, 276–292.
963 Muller, M., Verhagen, J.H.G., 2002a. Optimization of the mechanical performance of a
964 two-duct semicircular duct system—Part 1: dynamics and duct dimensions. J. Theor.
965 Biol. 216, 409–424.
966 Muller, M., Verhagen, J.H.G., 2002b. Optimization of the mechanical performance of a
967 two-duct semicircular duct system—Part 2: excitation of endolymph movements. J.
968 Theor. Biol. 216, 425–442.
969 Muller, M., Verhagen, J.H.G., 2002c. Optimization of the mechanical performance of a
970 two-duct semicircular duct system—Part 3: the positioning of the ducts in the head. J.
971 Theor. Biol. 216, 443–459.

Nengo, I., Tafforeau, P., Gilbert, C.C., Fleagle, J.G., Miller, E.R., Feibel, C., Fox, D.L., Feinberg, J., Pugh, K.D., Berruyer, C., Mana, S., Engle, Z., Spoor, F., 2017. New infant cranium from the African Miocene sheds light on ape evolution. Nature 548, 169–174.

Pagel, M., 1999. Inferring the historical patterns of biological evolution. Nature 401, 877–884.

Perier, A., Lebrun, R., Marivaux, L., 2016. Different level of intraspecific variation of the bony labyrinth morphology in slow- versus fast-moving Primates. J. Mammal. Evol. 23, 353–368.

R Core Team, 2019. R: A language and environment for statistical computing. R Foundation for Statistical Computing, Vienna.

Rae, T.C., Johnson, P.M., Yano, W., Hirasaki, E. 2016. Semicircular canal size and locomotion in colobine monkeys: a cautionary tale. Folia Primatol. 87, 213–223.

Revell, L.J., 2012. Phytools: an R package for phylogenetic comparative biology (and other things). Methods Ecol. Evol. 3, 217–223.

Rook, L., Renne, P., Benvenuti, M., Papini, M., 2000. Geochronology of *Oreopithecus*-bearing succession at Baccinello (Italy) and the extinction pattern of european miocene hominoids. J. Hum. Evol. 39, 577–582.

Rook, L., Bondioli, L., Casali, F., Rossi, M., Köhler, M., Moyá Solá, S., Macchiarelli, R., 2004. The bony labyrinth of *Oreopithecus bambolii*. J. Hum. Evol. 46, 347–354.

Rose, M.D., 1994. Quadrupedalism in some Miocene catarrhines. J. Hum. Evol. 26, 387–411.

Russo, G.A., 2016. Comparative sacral morphology and the reconstructed tail lengths of five extinct primates: *Proconsul heseloni*, *Epipliopithecus vindobonensis*, *Archaeolemur edwardsi*, *Megaladapis grandidieri*, and *Palaeopropithecus kelyus*. J. Hum. Evol. 90, 135–162.

998 Ryan, T.M., Silcox, M.T., Walker, A., Mao, X., Begun, D.R., Benefit, B.R., Gingerich, P.D.,
999 Köhler, M., Kordos, L., McCrossin, M.L., Moyà-Solà, S., Sanders, W.J., Seiffert, E.R.,
1000 Simons, E., Zalmout, I.S., Spoor, F., 2012. Evolution of locomotion in Anthropoidea:
1001 the semicircular canal evidence. P. Roy. Soc. B. 279, 3467–3475.
1002 Sankhyan, A. R., Kelley, J., & Harrison, T. 2017. A highly derived pliopithecoid from the
1003 Late Miocene of Haritalyangar, India. Journal of Human Evolution 105, 1–12.
1004 Savje, F. 2019. distances: tools for distance metrics. https://cran.r-
1005 project.org/web/packages/distances/index.html.
1006 Schlager, S., 2017. Morpho and Rvcg – shape analysis in R: R-packages for geometric
1007 morphometrics, shape analysis and surface manipulations. In: Zheng, G., Li, S.,
1008 Székely, G. (Eds.), Statistical Shape and Deformation Analysis. Methods,
1009 Implementation and Applications. Academic Press, London, pp. 217–256.
1010 Seiffert, E.R., 2006. Revised age estimates for the later Paleogene mammal faunas of
1011 Egypt and Oman. Proc. Natl. Acad. Sci. USA 103, 5000–5005.
1012 Sidlauskas, B., 2008. Continuous and arrested morphological diversification in sister
1013 clades of characiform fishes: a phylomorphospace approach. Evolution 62, 3135–
1014 3156.
1015 Silcox, M.T., Bloch, J.I., Boyer, D.M., Godinot, M., Ryan, T.M., Spoor, F., Walker, A., 2009.
1016 Semicircular canal system in early primates. J. Hum. Evol. 56, 315–327.
1017 Simons, E.L., Fleagle, J.G., 1973. The history of extinct gibbon-like primates. In:
1018 Rumbaugh, D.M. (Ed.), Gibbon and Siamang Vol. 2. Anatomy, Dentition, Taxonomy,
1019 Molecular Evolution and Behavior. Karger, Basel, pp. 121–148.
1020 Simons, E.L., Seiffert, E.R., Ryan, T.M., Attia, Y., 2007. A remarkable female cranium of
1021 the early Oligocene anthropoid *Aegyptopithecus zeuxis* (Catarrhini, Propliopithecidae).
1022 Proc. Natl. Acad. Sci. USA 104, 8731–8736.

1023 Spoor, F., Zonneveld., F., 1998. Comparative review of the human bony labyrinth. Yearb.
1024 Phys. Anthropol. 41, 211–251.
1025 Spoor, F., Garland, T., Krovitz, G., Ryan, T.M., Silcox, M.T., Walker, A., 2007. The primate
1026 semicircular canal system and locomotion. Proc. Natl. Acad. Sci. USA 104, 10808–
1027 10812.
1028 Stevens, N.J., Seiffert, E.R., O'Connor, P.M., Roberts, E.M., Schmitz, M.D., Krause, C.,
1029 Gorscak, E., Ngasala, S., Hieronymus, T.L., Temu, J., 2013. Palaeontological
1030 evidence for an Oligocene divergence between Old World monkeys and apes. Nature
1031 497, 611–614.
1032 Swofford, D., 2003. PAUP*. Phylogenetic Analysis Using Parsimony (*and Other
1033 Methods). Version 4. Sinauer Associates, Sunderland.
1034 Szalay, F.S., 1975. Phylogeny of primate higher taxa: the basicranial evidence. In: Luckett,
1035 W.P., Szalay, F.S. (Eds.), Phylogeny of the Primates: A Multidisciplinary Approach.
1036 Plenum Press, New York, pp. 91–125.
1037 Szalay, F.S., Delson, E., 1979. Evolutionary History of the Primates. Academic Press, New
1038 York.
1039 Tejedor, M.F., Rosenberger, A.L., 2008. A neotype for *Homunculus patagonicus*
1040 Ameghino, 1891, and a new interpretation of the taxon. PaleoAnthropology 2008, 68–
1041 82.
1042 Urciuoli, A., Zanolli, C., Begun, D.R., Almécija, S., Dumoncel, J., Moyà-Solà, S., Alba,
1043 D.M., 2019. A deformation-based geometric morphometric analysis of the vestibular
1044 apparatus in the Miocene apes *Hispanopithecus laietanus* and *Rudapithecus*
1045 *hungaricus*. Am. J. Phys. Anthropol. 168 (S68), 253.
1046 Urciuoli, A., Zanolli, C., Beaudet, A., Dumoncel, J., Santos, F., Moyà-Solà, S., Alba, D.M.,
1047 2020. The evolution of the vestibular apparatus in apes and humans. eLife 9, e51261.

van der Meulen, A.J., García-Paredes, I., Álvarez-Sierra, M.Á., van den Hoek Ostende, L.W., Hordijk, K., Oliver, A., López-Guerrero, P., Hernández-Ballarín, V., Peláez-Campomanes, P., 2011. Biostratigraphy or biochronology? Lessons from the Early and Middle Miocene small Mammal Events in Europe. Geobios 44, 309–321.

Zalmout, I.S., Sanders, W.J., MacLatchy, L., Gunnell, G., Al-Mufarreh, Y.A., Ali, M.A., Nasser, A.-A. H., Al-Masary, A.M., Al-Sobhi, S.A., Nadhra, A.O., Matari, A.H., Wilson, J. A., Gingerich, P. D., 2010. New Oligocene primate from Saudi Arabia and the divergence of apes and Old World monkeys. Nature 466, 360–365.

Zapfe, H., 1958. The skeleton of *Pliopithecus* (*Epipliopithecus*) *vindobonensis* Zapfe and Hürzeler. Am. J. Phys. Anthropol. 16, 441–457.

Zapfe, H., 1961. Die Primatenfunde aus der miozänen Spaltenfüllung von Neudorf an der March (Děvínská Nová Ves), Tschechoslowakei. Schweizer. palaeontol. Abh. 78, 1–293.

Zapfe, H., Hürzeler, J., 1957. Die Fauna der miozänen Spaltenfüllung von Neudorf an der March (ČSR.). Primates. Sitzungsber. Öst. Akad. Wiss. Math. Naturwiss. Kl. 166, 113–123.

Table 1. Digital object identifiers (DOIs) of the 3D virtual models of the vestibule and semicircular canals of *Epipliopithecus vindobonensis* available from MorphoSource.org (https://www.morphosource.org).

Catalog No.	Museum	DOI
NMBOE 303a (individual III)	NMBOE	https://doi.org/10.17602/M2/M113935
NMBOE 303b (individual III)	NMBOE	https://doi.org/10.17602/M2/M113933
NHMW 1970/1397/0003 (individual II)	NHMW	https://doi.org/10.17602/M2/M113932

Abbreviations: NMB OE = Naturhistorisches Museum Basel, Switzerland; NHMW = Naturhistorisches Museum Wien, Austria.

Table 2. Log-transformed cube root of canal volume (ln VolSC, mm^3) and log-transformed canal length (ln L, mm) measured for the fossil taxa included in the analysis.[a]

Catalog No.	Taxon	ln VolSC	ln L
NMBOE 303a	*Epipliopithecus vindobonensis*	3.640	0.993
NMBOE 303b	*Epipliopithecus vindobonensis*	3.602	0.910
NHMW 1970/1397/0003	*Epipliopithecus vindobonensis*	3.593	0.916
CGM 85785	*Aegyptopithecus zeuxis*	3.365	0.847
MPM-PV 30501	*Homunculus patagonicus*	3.391	0.780
MPM-PV 30502	*Homunculus patagonicus*	3.359	0.720
MPM-PV 30503	*Homunculus patagonicus*	3.359	0.784
MACN 14128	*Dolichocebus gaimanensis*	3.802	0.803
BAC 208	*Oreopithecus bambolii*	3.295	0.803
DPC 18651	*Parapithecus grangeri*	3.640	0.993

Abbreviations: BAC = Baccinello (field acronym; housed at Naturhistorisches Museum Basel, Switzerland); CGM = Egyptian Geological Museum, Cairo, Egypt; MPM-PV = Museo Regional Provincial Padre M.J. Molina, Río Gallegos, Argentina; MACN = Museo Argentino de Ciencias Naturales, Buenos Aires, Argentina; DPC = Duke Lemur Center, Durham, NC, USA.

a See SOM Table S1 for the specimens included in the extant comparative sample.

Table 3. Mahalanobis distances (D^2) and posterior probabilities of group membership (*p*) based on the scores for fossil specimens in the between-group principal component analysis for the entire anthropoid sample.[a,b]

D^2	Cercopithecoidea	Hominidae	Hylobatidae	Platyrrhini
Epipliopithecus vindobonensis (NHMW 1970/1397/0003)	17.179	10.539	6.485	**3.437**
Epipliopithecus vindobonensis (NMB OE 303a)	12.190	14.262	6.588	**0.779**
Epipliopithecus vindobonensis (NMB OE 303b)	13.307	15.085	6.682	**1.056**
Oreopithecus bambolii (BAC 208)	8.083	5.450	11.574	**1.579**
Aegyptopithecus zeuxis (CGM 85785)	12.430	9.133	15.513	**0.990**
Homunculus patagonicus (MPM-PV 3501)	11.817	13.356	11.017	**0.073**
Homunculus patagonicus (MPM-PV 3502)	10.336	12.736	12.056	**0.165**
Homunculus patagonicus (MPM-PV 3503)	10.083	7.449	11.284	**0.590**
Dolichocebus gaimanensis (MACN 14128)	5.204	13.516	12.687	**1.935**
Parapithecus grangeri (DPC 18651)	6.533	17.859	13.047	**2.110**
P	Cercopithecoidea	Hominidae	Hylobatidae	Platyrrhini
Epipliopithecus vindobonensis (NHMW 1970/1397/0003)	0.006	0.007	0.018	**0.029**
Epipliopithecus vindobonensis (NMB OE 303a)	0.018	<0.001	<0.001	**0.678**
Epipliopithecus vindobonensis (NMB OE 303b)	0.013	<0.001	<0.001	**0.608**
Oreopithecus bambolii (BAC 208)	0.052	0.005	<0.001	**0.530**
Aegyptopithecus zeuxis (CGM 85785)	0.001	<0.001	<0.001	**0.688**
Homunculus patagonicus (MPM-PV 3501)	0.003	<0.001	<0.001	**0.980**
Homunculus patagonicus (MPM-PV 3502)	0.003	<0.001	<0.001	**0.919**
Homunculus patagonicus (MPM-PV 3503)	0.019	0.001	<0.001	**0.848**

D^2	Cercopithecoidea	Hominidae	Hylobatidae	Platyrrhini
Dolichocebus gaimanensis (MACN 14128)	0.013	<0.001	<0.001	**0.612**
Parapithecus grangeri (DPC 18651)	0.002	<0.001	<0.001	**0.411**

Abbreviations: NHMW = Naturhistorisches Museum of Wien, Austria; NMB = Naturhistorisches Museum of Basel, Switzerland; BAC = NMB accession number for *Oreopithecus bambolii* specimens; CGM = Egyptian Geological Museum, Cairo, Egypt; MPM-PV = Museo Regional Provincial Padre M.J. Molina, Río Gallegos, Argentina; MACN = Museo Argentino de Ciencias Naturales, Buenos Aires, Argentina; DPC = Duke Lemur Center, Durham, NC, USA.

a

Note that these are probability estimates of having a particular score given membership in a particular group, not the likelihood of group membership in each of the a priori defined groups given a particular score (the greater the number, the higher the probability).

b

The lowest distance (D^2) and highest posterior probability of group membership (*p*) for each specimen are bolded.

Table 4. Mahalanobis distances (D^2) and posterior probabilities of group membership (*p*) based on the scores for fossil specimens in the between-group principal component analysis for the entire anthropoid sample and considering all catarrhines as a single group.[a,b]

D^2	Catarrhini	Platyrrhini
Epipliopithecus vindobonensis (NHMW 1970/1397/0003)	13.016	**5.341**
Epipliopithecus vindobonensis (NMB OE 303a)	11.837	**1.654**
Epipliopithecus vindobonensis (NMB OE 303b)	13.040	**2.098**
Oreopithecus bambolii (BAC 208)	9.085	**3.890**
Aegyptopithecus zeuxis (CGM 85785)	16.900	**3.204**
Homunculus patagonicus (MPM-PV 3501)	13.814	**0.135**
Homunculus patagonicus (MPM-PV 3502)	13.057	**0.284**
Homunculus patagonicus (MPM-PV 3503)	10.989	**1.806**
Dolichocebus gaimanensis (MACN 14128)	8.645	**2.417**
Parapithecus grangeri (DPC 18651)	12.592	**3.670**
P	Catarrhini	Platyrrhini
Epipliopithecus vindobonensis (NHMW 1970/1397/0003)	0.109	**0.241**
Epipliopithecus vindobonensis (NMB OE 303a)	0.022	**0.876**
Epipliopithecus vindobonensis (NMB OE 303b)	0.017	**0.847**
Oreopithecus bambolii (BAC 208)	0.124	**0.673**
Aegyptopithecus zeuxis (CGM 85785)	0.002	**0.886**
Homunculus patagonicus (MPM-PV 3501)	0.002	**0.985**
Homunculus patagonicus (MPM-PV 3502)	0.002	**0.968**
Homunculus patagonicus (MPM-PV 3503)	0.034	**0.935**
Dolichocebus gaimanensis (MACN 14128)	0.013	**0.841**
Parapithecus grangeri (DPC 18651)	0.002	**0.795**

Abbreviations: NHMW = Naturhistorisches Museum of Wien, Austria; NMB = Naturhistorisches Museum of Basel, Switzerland; BAC = NMB accession number for *Oreopithecus bambolii* specimens; CGM = Egyptian Geological Museum, Cairo, Egypt; MPM-PV = Museo Regional Provincial Padre M.J. Molina, Río Gallegos, Argentina; MACN = Museo Argentino de Ciencias Naturales, Buenos Aires, Argentina; DPC = Duke Lemur Center, Durham, NC, USA.

a

Note that these are probability estimates of having a particular score given membership in a particular group, not the likelihood of group membership in each of the a priori defined groups given a particular score (the greater the number, the higher the probability).

b

The lowest distance and highest probability for each specimen are bolded.

Table 5. Mahalanobis distances (D^2) between specimens of *Epipliopithecus* and other fossils based on between group principal component analysis scores.

D^2	NHMW 1970/1397/0003	NMB OE 303a	NMB OE 303b
Epipliopithecus vindobonensis (NHMW 1970/1397/0003)	–	1.332	1.285
Epipliopithecus vindobonensis (NMB OE 303a)	1.332	–	0.176
Epipliopithecus vindobonensis (NMB OE 303b)	1.285	0.176	–
Oreopithecus bambolii (BAC 208)	2.244	1.901	2.055
Aegyptopithecus zeuxis (CGM 85785)	2.360	1.804	1.927
Homunculus patagonicus (MPM-PV 3501)	1.943	0.919	1.033
Homunculus patagonicus (MPM-PV 3502)	2.246	1.251	1.388
Homunculus patagonicus (MPM-PV 3503)	1.914	1.450	1.592
Dolichocebus gaimanensis (MACN 14128)	3.081	2.077	2.243
Parapithecus grangeri (DPC18651)	3.201	2.017	2.161

Abbreviations: NHMW = Naturhistorisches Museum Wien, Austria; NMB OE = Naturhistorisches Museum Basel, Switzerland; BAC = Baccinello (housed at NMB); CGM = Egyptian Geological Museum, Cairo, Egypt; MPM-PV = Museo Regional Provincial Padre M.J. Molina, Río Gallegos, Argentina; MACN = Museo Argentino de Ciencias Naturales, Buenos Aires, Argentina; DPC = Duke Lemur Center, Durham, NC, USA.

Table 6. Phylogenetic signal computed for the between-group principal analysis applied to the deformation fields of the extant anthropoid comparative sample. The variance explained by each principal component (bgPC) and the *p*-value for the statistics are given within parentheses.

	bgPC1 (59%)	**bgPC2 (30%)**	**bgPC3 (11%)**
Pagel's λ	1.000 ($p < 0.0001$)	0.843 ($p < 0.0001$)	0.925 ($p < 0.0001$)
Blomberg's K	1.148 ($p < 0.0001$)	1.446 ($p < 0.001$)	0.732 ($p < 0.001$)

Table 7. Weighted Euclidean distances computed between the between-group principal component scores of the reconstructed last common ancestors (LCAs) and the *Epipliopithecus* centroid.

LCA	Distance
Crown anthropoids	1.304
Crown platyrrhines	1.141
Crown catarrhines	0.989
Crown cercopithecoids	1.646
Crown hominoids	1.256

Table 8. Definition of the discrete characters of semicircular canal (SC) and vestibule morphology used in this paper.

Character No.	Character statements (characters + character states)[a]
#1	Size of the vestibule relative to the SCs: 0 = small; 1 = large.
#2	Robusticity of the SCs: 0 = slender; 1 = stout.
#3	Shape of the anterior SC: 0 = vertically compressed; 1 = rounded; 2 = elongated superiorly.
#4	Shape of the anterior portion of the anterior SC: 0 = non-projecting anterosuperiorly; 1 = anterosuperiorly projecting.
#5	Shape of the posterior SC: 0 = vertically compressed; 1 = rounded; 2 = elongated superiorly.
#6	Shape of the lateral SC ampullary portion: 0 = flat or only slightly bent superiorly; 1 = markedly bent superiorly.
#7	Length of the CC: 0 = long; 1 = intermediate; 2 = short.

a See Figure 11 for an illustration of the character states.

Table 9. Character states coded for the estimated last common ancestors (LCAs) and for the fossil taxa included in the analysis.[a].

Species/LCAs	#1	#2	#3	#4	#5	#6	#7
Epipliopithecus vindobonensis	0	0	1	0	2	0	0
Aegyptopithecus zeuxis	0	0	2	0	2	0	0
Dolichocebus gaimanensis	0	0	2	0	2	0	0
Homunculus patagonicus	0	0	2	0	0, 2	0	0
Oreopithecus bambolii	1	1	0	1	1	0	2
Parapithecus grangeri	0	0	2	0	2	0	0
Crown anthropoid LCA	0	0	2	0	2	0	0
Crown platyrrhine LCA	0	0	2	0	2	0	0
Crown catarrhine LCA	0	0	1	0	1	0	1
Crown cercopithecoid LCA	0	0	1	0	1	0	1
Crown hominoid LCA	0	0	0	0	1	1	2
Crown hylobatid LCA	0	0	0	1	1	1	2
Crown hominid LCA	1	1	0	0	1	1	2

a

See character definitions in Table 7 and SOM Table S2 for the coding of extant species.

Table 10. Measures of character congruence for the two main phylogenetic hypotheses (i.e., stem catarrhine vs. stem hominoid) discussed in this paper for *Epipliopithecus*. The higher the index, the more parsimonious the hypothesis.[a].

Metrics	Stem catarrhine (Fig. 3a)	Stem hominoid (Fig. 3b)
Tree length	22	24
CI	0.455	0.417
RI	0.826	0.797
RC	0.376	0.332

Abbreviations: CI = consistency index; RI = retention index; RC = rescaled consistency index.

a See also Figure 3 and SOM Table 2 for character descriptions.

Figure captions

Figure 1. Illustration of the protocol used for digitally separating the cochlea (green) from the semicircular canals and the vestibule (blue). a) In anterior view, the first landmark (yellow filled circle) is placed anteriorly to the oval window, on the point of maximum surface curvature of the ridge-like morphology formed by the narrowing of the vestibule. b) In posterior view, three landmarks are placed along the junction between the bony vestibule and the cochlea, defined by the line of maximum surface curvature found immediately below the bulge formed by the saccular recess. A cutting plane (here perpendicular to the view and depicted by a black line) is best fitted to the identified landmarks using the 'Points To Fit' option of the 'Clipping Plane' module of Avizo version 9.0.1 (FEI Visualization Sciences Group, Houston) via a customized script (available upon request to A.U.), and used as a reference for a straight cut. Abbreviations: asc = anterior semicircular canal; psc = posterior semicircular canal; lsc = lateral semicircular canal; CC = common crus.

Figure 2. Cladogram of extant and fossil anthropoids showing the two phylogenetic hypotheses for *Epipliopithecus*. The solid line (A) denotes the most widely accepted phylogenetic position of *Epipliopithecus* as a stem catarrhine, whereas the dashed line (B) denotes the alternative hypothesis that *Epipliopithecus* would be more closely related to hominoids. Key nodes are highlighted as follows: gray circle = crown anthropoids; green circle = crown platyrrhines; blue circle = crown catarrhines; orange circle = crown hominoids. Skulls and crania (not to scale) were taken from the following sources for illustrative purposes only: extant skulls and *Aegyptopithecus*, Wikimedia Commons; *Dolichocebus*, Kay et al. (2009b: Fig. 1); *Homunculus*, Tejedor and Rosenberger (2008: Fig. 2); *Oreopithecus* (reconstruction), Moyà-Solà and Köhler (2000: Fig. 5);

Epipliopithecus, photograph of a cast; *Parapithecus*, digital reconstruction with photographic texture made by Steven Heritage.

Figure 3. Phylogenetic trees used for the phylomorphospace approach. They differ in considering *Epipliopithecus* as a stem catarrhine (a) or a stem hominoid (b).

Figure 4. Rendered 3D models of the semicircular canals and vestibule of *Epipliopithecus vindobonensi*s (all specimens depicted as from the left side) and selected extant anthropoids, in lateral (left), superior (middle), and posterior (right) views: a) *E. vindobonensis* (individual II, NHMW 1970/1397/0003, mirrored); b) *E. vindobonensis* (individual III, NMB OE 303a); c) *E. vindobonensis* (individual III, NMB OE 303b, mirrored); d) *Parapithecus grangeri* (DPC 18651); e) *Dolichocebus gaimanensis* (MACN 14128); f) *Homunculus patagonicus* (MPM-PV 3501); g) *Ateles geoffroyi* (MCZ 29628); h) *Alouatta palliata* (DU EA LP12); i) *Cebus apella* (MCZ27891); j) *Aegyptopithecus zeuxis* (CGM 85785); k) *Trachypithecus cristatus* (MCZ35603); l) *Chlorocebus pygerythrus* (SIU 4796); m) *Macaca fascicularis* (MCZ 35765); n) *Oreopithecus bambolii* (BAC 208); o) *Hylobates lar* (MCZ 41424); p) *Symphalangus syndactylus* (AMNH.M 106583); q) *Hoolock hoolock* (AMNH.M 83425); r) *Pongo pygmaeus* (IPS10647); s) *Gorilla gorilla* (AMNH.M 167338; t) *Pan paniscus* (MCZ 38019); u) *Homo sapiens* (EMBR 179). Scale bars equal 5 mm.

Figure 5. Bivariate plot of canal log-transformed cube root canal volume (mm; Ln VolSC) vs. log-transformed canal length (mm; ln L). Separate regression lines are depicted for hominids (red line) and for nonhominid anthropoids (blue line). *Epipliopithecus* (NHMW 1970/1397/0003 and NMB OE 303a, b) falls within the variability of nonhominid anthropoids, similar to all extinct taxa except *Oreopithecus*. Measurements for the included fossil taxa given in Table 6.

Figure 6. Patterns of vestibule and semicircular canal shape variation among major anthropoid clades based on the results of a between-group principal component analysis, as depicted by bivariate plots between principal components (bgPCs): a) bgPC2 vs. bgPC1; b) bgPC3 vs. bgPC1. Variance explained by each component is given along each axis. c–e) Extreme conformations of maximum (above) and minimum (below) bgPC scores: c) bgPC1; d) bgPC2; e) bgPC3. Four groups (platyrrhines, cercopithecoids, hylobatids, and hominids) were defined a priori, whereas specimens of *Epipliopithecus vindobonensis* were plotted post hoc onto the morphospace. Renderings in lateral (left), superior (middle), and posterior (right) views of warped 3D models representing the extreme conformations for each bgPC are placed close to the corresponding axis. Convex hulls depict the range of variation for a priori defined groups using the following color code: green = platyrrhines; blue = cercopithecoids; red = hylobatids; orange = hominids.

Figure 7. Dendrogram resulting from a cluster analysis (Ward's method) based on Mahalanobis distances computed between the species centroids of the between-group principal component analysis (bgPCA) of shape data. The cophenetic correlation coefficient is 0.703.

Figure 8. Phylomorphospace of the anthropoid semicircular canal. The phylogenetic tree (with *Epipliopithecus* included as a stem catarrhine; Fig. 3a) is projected onto the tangent space defined by the between-group principal components (bgPCs) as depicted in Figure 6. The internal nodes (i.e., the ancestral states) were estimated using maximum likelihood: a) bgPC2 vs. bgPC1; b) bgPC3 vs. bgPC1. Variance explained by each component is given along each axis. Convex hulls depict the range of variation for a priori defined groups using the following color code: green = platyrrhines; blue = cercopithecoids; red =

hylobatids; orange = hominids. The ancestral nodes discussed for assessing *Epipliopithecus* phylogenetic affinities do not change consistently in their position in the morphospace irrespective of the phylogenetic hypothesis used for their estimation (see SOM Fig. S3 for the alternative phylogenetic tree including *Epipliopithecus* as a stem hominoid). Key nodes are highlighted as follows: gray circle = crown anthropoids; green circle = crown platyrrhines; blue circle = crown catarrhines; orange circle = crown hominoids.

Figure 9. Reconstruction of the semicircular canals and vestibule for the last common ancestors (LCAs) of the following clades: a) crown anthropoids; b) crown platyrrhines; c) crown catarrhines; d) crown hominoids. The renderings of each 3D model are depicted in lateral (left), superior (middle), and posterior (right) views.

Figure 10. Box-and-whisker plot of allometric residuals based on best-fit line of the nonhominid anthropoid regression of log-transformed cube root of canal volume and log-transformed canal length (as depicted in Fig. 5). Vertical lines correspond to the median, boxes depict interquartile range, whiskers represent maximum and minimum values within 1.5 times the interquartile range, and black dots are outliers. Sample sizes for extant groups are the following: Platyrrhini (n = 40), Cercopithecoidea (n = 75), Hylobatidae (n = 17), Hominidae (n = 30).

Figure 11. Illustration of the discrete characters of semicircular canal (SC) and vestibule morphology used in this paper. Numbers preceding each state (0, 1, 2) correspond to character states numbered in Tables 8 and 9, and SOM Table S4.

Figure 12. Simplified cladogram of crown anthropoids and selected extinct catarrhines (*Epipliopithecus* and *Oreopithecus*) summarizing the main synapomorphies inferred for the various clades in semicircular canal and vestibule morphology. The four extant anthropoid clades distinguished (platyrrhines, cercopithecoids, hylobatids and hominids) are depicted as terminal nodes. The synapomorphies inferred for each node are summarized below; character number (preceded by a hash) and character state (within parentheses) are provided after each synapomorphy within brackets. a) *Epipliopithecus* + crown catarrhines: rounded anterior canal [#3(1)]; b) Crown catarrhines: rounded posterior canal [#5(1)], moderately short CC [#7(1)]; c) *Oreopithecus* + crown hominoids: vertically compressed anterior canal [#3(0)], anterosuperiorly-projecting anterior portion of the anterior canal [#4(1)], short CC [#7(2)]; d) Crown hominoids: markedly superiorly bent ampullary portion of the lateral canal [#6(1)]; e) Crown hominids (unless *Oreopithecus* + crown hominoid synapomorphies [node c] with reversal in hylobatids): large vestibule relative to the SCs [#1(1)], stout SCs [#2(1)]. Abbreviations: CC = common crus; SC = semicircular canals. See Figure 11 for an illustration of the various character states and Table 9 and SOM Table S4 for the scoring of reconstructed last common ancestors and individual taxa, respectively.

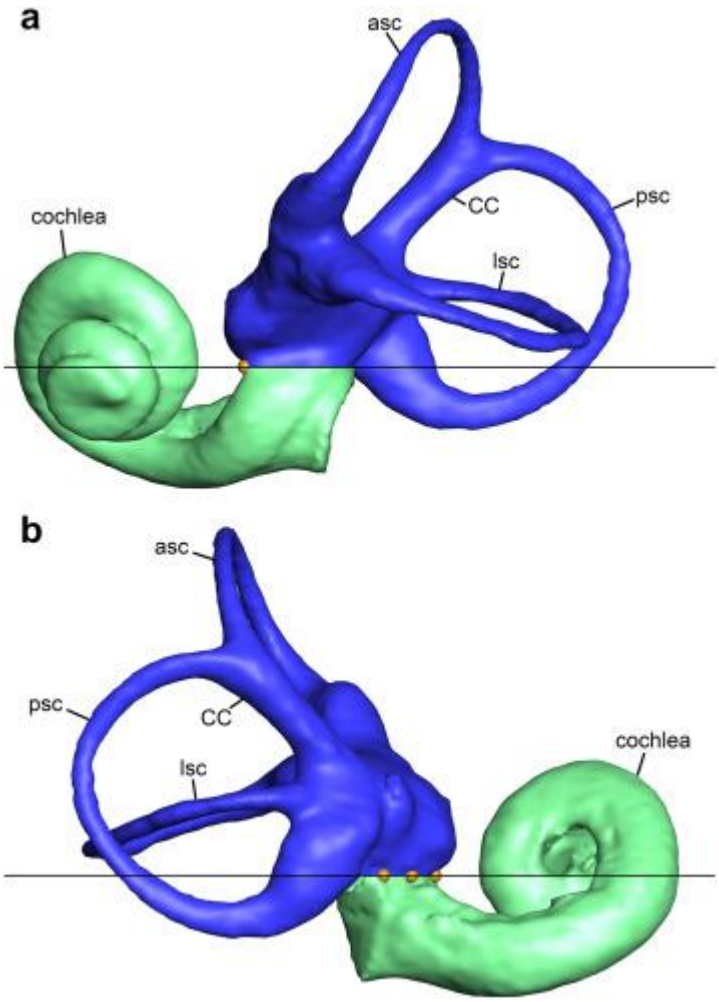

1262

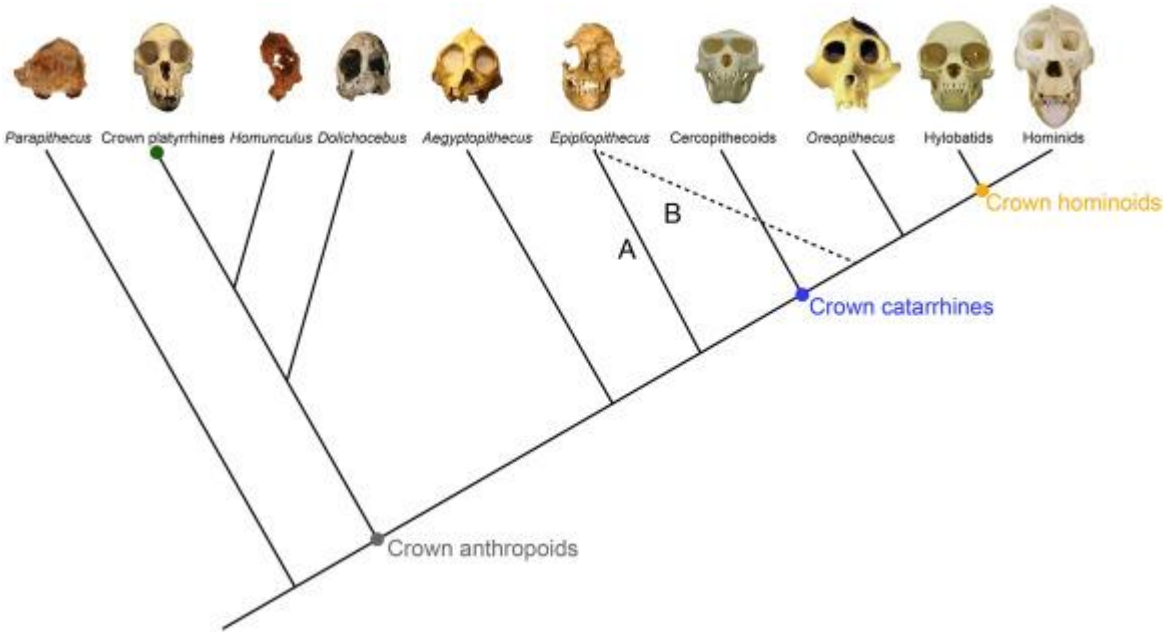
Parapithecus
Crown platyrrhines
Homunculus
Dolichocebus
Aegyptopithecus
Epipliopithecus
Cercopithecoids
Oreopithecus
Hylobatids
Hominids
Crown hominoids
B
A
Crown catarrhines
Crown anthropoids

1263

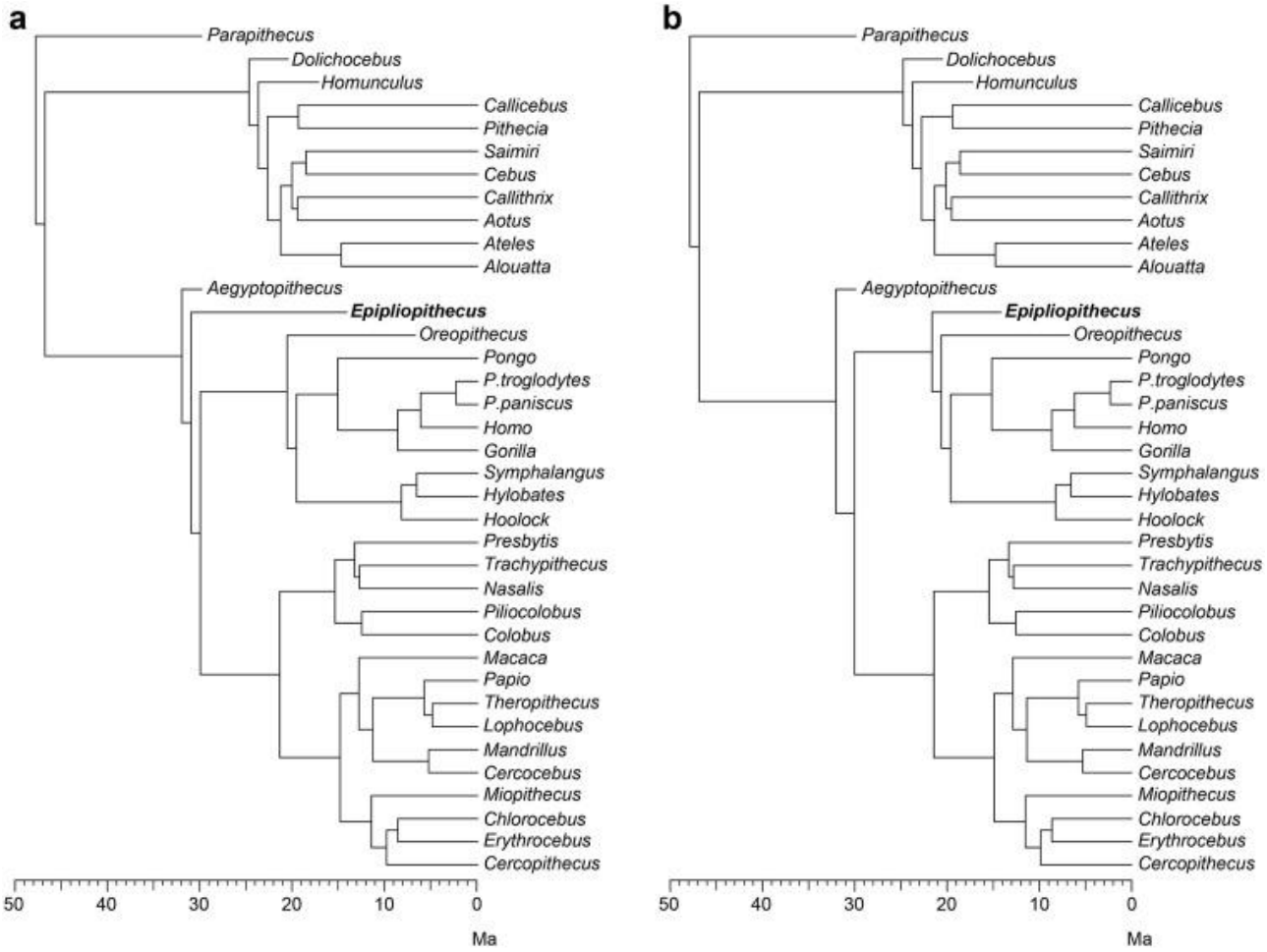
a
Parapithecus
Dolichocebus
Homunculus
Callicebus
Pithecia
Saimiri
Cebus
Callithrix
Aotus
Ateles
Alouatta
Aegyptopithecus
Epipliopithecus
Oreopithecus
Pongo
P.troglodytes
P.paniscus
Homo
Gorilla
Symphalangus
Hylobates
Hoolock
Presbytis
Trachypithecus
Nasalis
Piliocolobus
Colobus
Macaca
Papio
Theropithecus
Lophocebus
Mandrillus
Cercocebus
Miopithecus
Chlorocebus
Erythrocebus
Cercopithecus
50
40
30
20
10
0
Ma
b
Parapithecus
Dolichocebus
Homunculus
Callicebus
Pithecia
Saimiri
Cebus
Callithrix
Aotus
Ateles
Alouatta
Aegyptopithecus
Epipliopithecus
Oreopithecus
Pongo
P.troglodytes
P.paniscus
Homo
Gorilla
Symphalangus
Hylobates
Hoolock
Presbytis
Trachypithecus
Nasalis
Piliocolobus
Colobus
Macaca
Papio
Theropithecus
Lophocebus
Mandrillus
Cercocebus
Miopithecus
Chlorocebus
Erythrocebus
Cercopithecus
50
40
30
20
10
0
Ma

1264

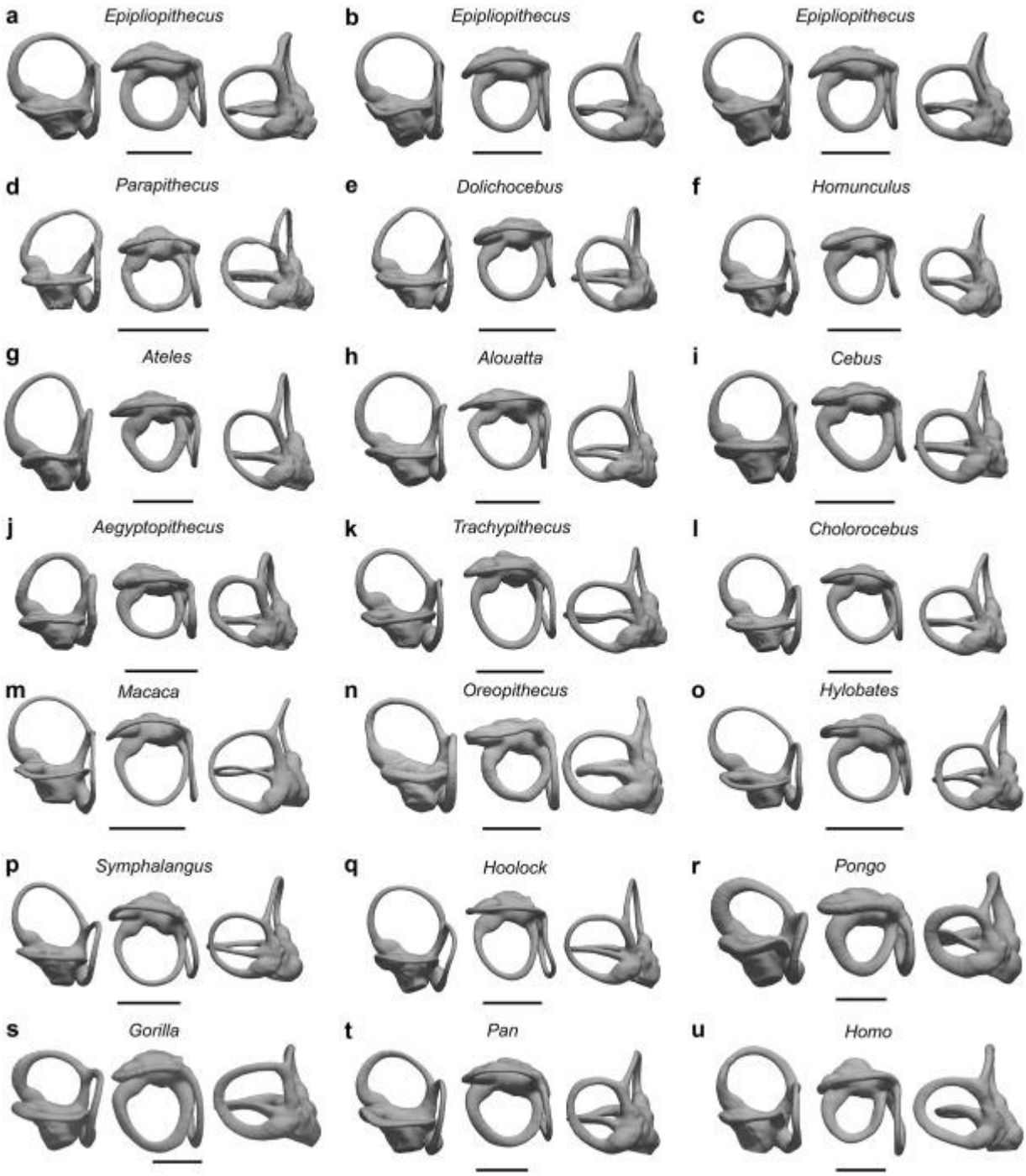
a Epipliopithecus
b Epipliopithecus
c Epipliopithecus
d Parapithecus
e Dolichocebus
f Homunculus
g Ateles
h Alouatta
i Cebus
j Aegyptopithecus
k Trachypithecus
l Cholorocebus
m Macaca
n Oreopithecus
o Hylobates
p Symphalangus
q Hoolock
r Pongo
s Gorilla
t Pan
u Homo

1265

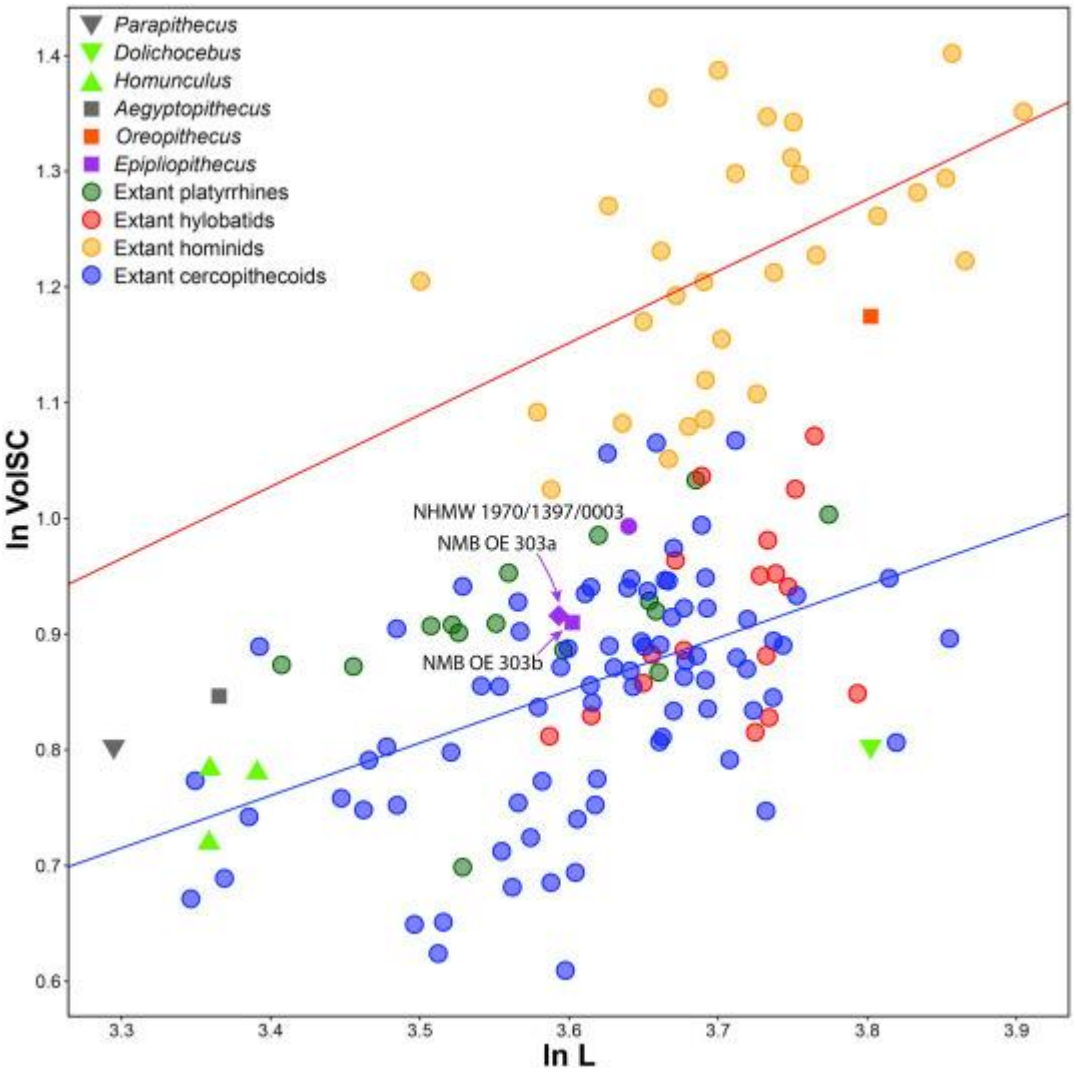
Parapithecus
Dolichocebus
Homunculus
Aegyptopithecus
Oreopithecus
Epipliopithecus
Extant platyrrhines
Extant hylobatids
Extant hominids
Extant cercopithecoids
NHMW 1970/1397/0003
NMB OE 303a
NMB OE 303b
ln VolSC
ln L
1.4
1.3
1.2
1.1
1.0
0.9
0.8
0.7
0.6
3.3
3.4
3.5
3.6
3.7
3.8
3.9

1266

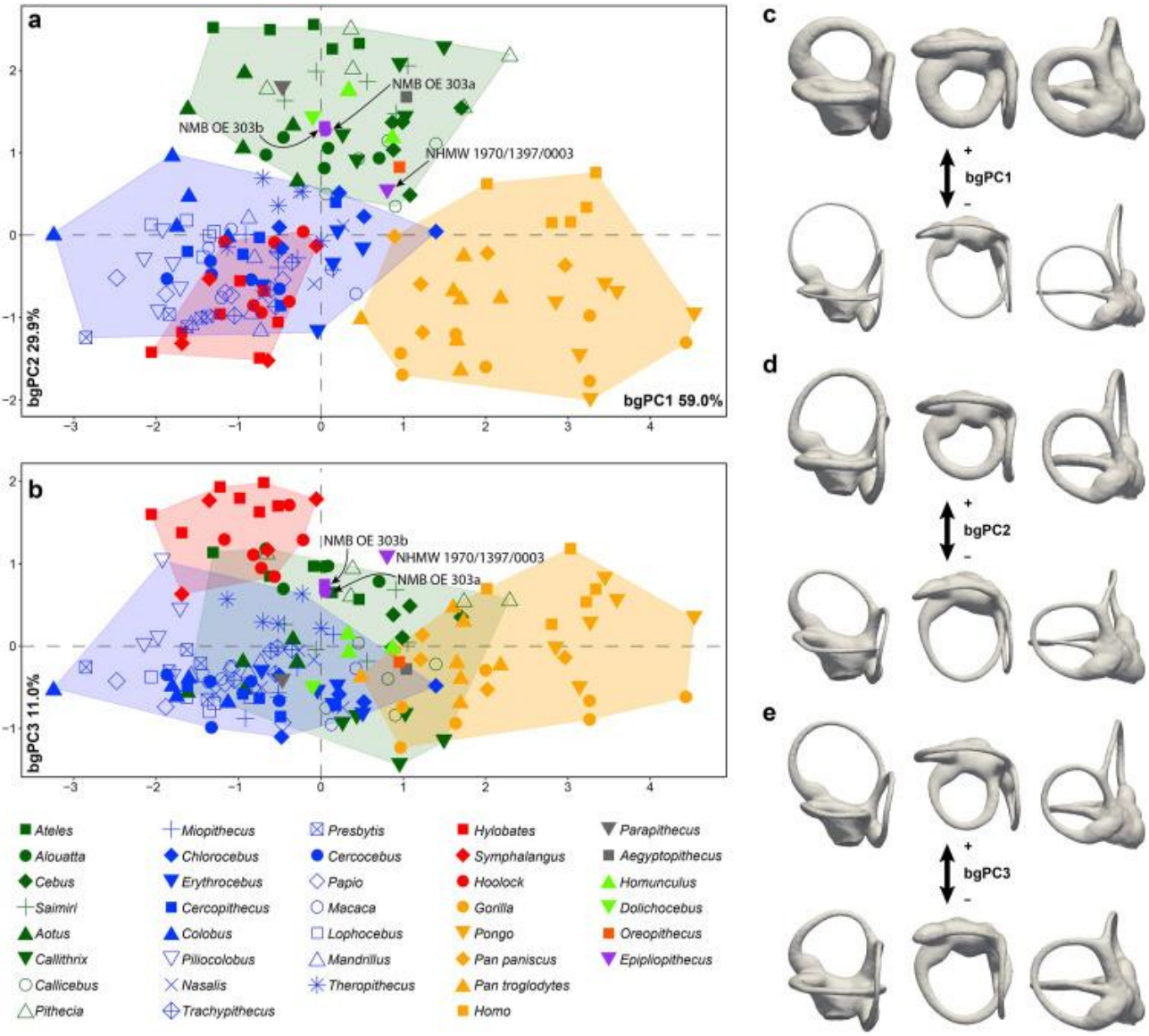
a
NMB OE 303a
NMB OE 303b
NHMW 1970/1397/0003
bgPC2 29.9%
bgPC1 59.0%
b
NMB OE 303b
NHMW 1970/1397/0003
NMB OE 303a
bgPC3 11.0%
Ateles
Alouatta
Cebus
Saimiri
Aotus
Callithrix
Callicebus
Pithecia
Miopithecus
Chlorocebus
Erythrocebus
Cercopithecus
Colobus
Piliocolobus
Nasalis
Trachypithecus
Presbytis
Cercocebus
Papio
Macaca
Lophocebus
Mandrillus
Theropithecus
Hylobates
Symphalangus
Hoolock
Gorilla
Pongo
Pan paniscus
Pan troglodytes
Homo
Parapithecus
Aegyptopithecus
Homunculus
Dolichocebus
Oreopithecus
Epipliopithecus
c
bgPC1
d
bgPC2
e
bgPC3

1267

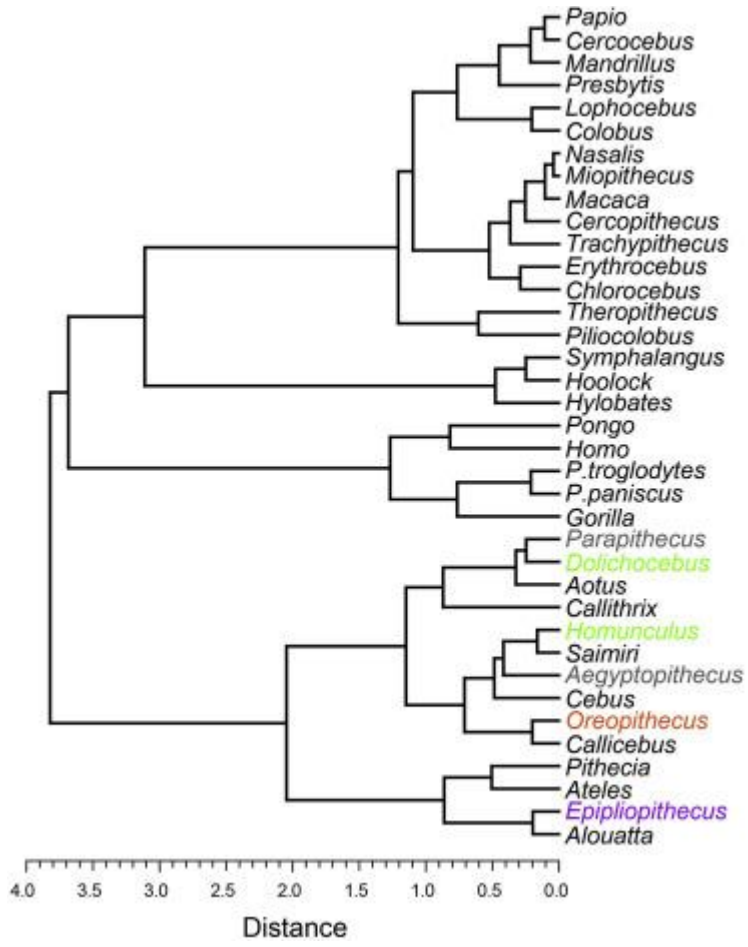
Papio
Cercocebus
Mandrillus
Presbytis
Lophocebus
Colobus
Nasalis
Miopithecus
Macaca
Cercopithecus
Trachypithecus
Erythrocebus
Chlorocebus
Theropithecus
Piliocolobus
Symphalangus
Hoolock
Hylobates
Pongo
Homo
P.troglodytes
P.paniscus
Gorilla
Parapithecus
Dolichocebus
Aotus
Callithrix
Homunculus
Saimiri
Aegyptopithecus
Cebus
Oreopithecus
Callicebus
Pithecia
Ateles
Epipliopithecus
Alouatta
4.0
3.5
3.0
2.5
2.0
1.5
1.0
0.5
0.0
Distance

1268

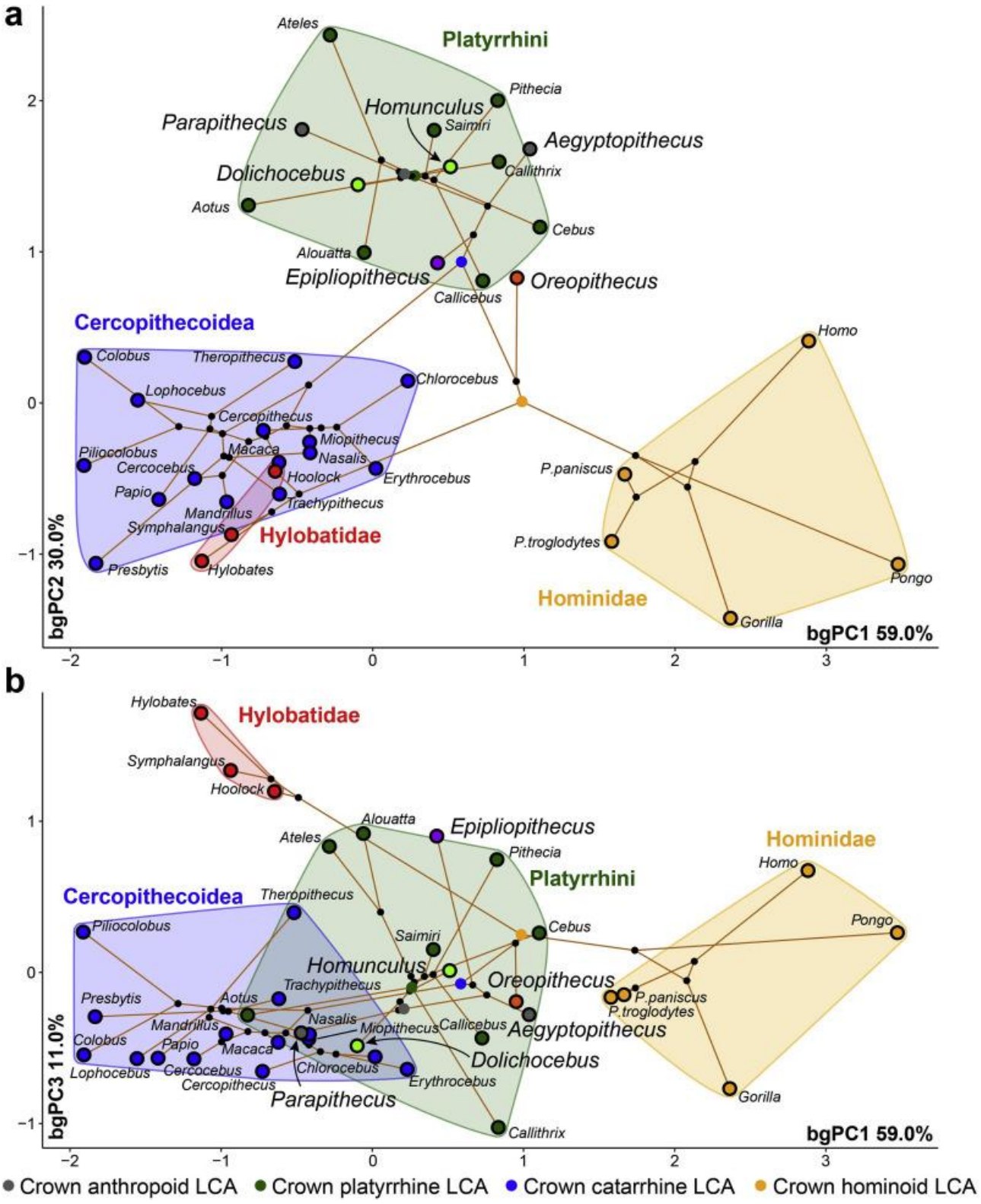
a
Platyrrhini
Cercopithecoidea
Hylobatidae
Hominidae
Ateles
Pithecia
Homunculus
Saimiri
Parapithecus
Aegyptopithecus
Dolichocebus
Callithrix
Aotus
Cebus
Alouatta
Epipliopithecus
Oreopithecus
Callicebus
Homo
Colobus
Theropithecus
Chlorocebus
Lophocebus
Cercopithecus
Miopithecus
Piliocolobus
Macaca
Nasalis
Cercocebus
Hoolock
Erythrocebus
P.paniscus
Papio
Trachypithecus
Mandrillus
Symphalangus
P.troglodytes
Presbytis
Hylobates
Pongo
Gorilla
bgPC2 30.0%
bgPC1 59.0%
b
Hylobates
Hylobatidae
Symphalangus
Hoolock
Alouatta
Epipliopithecus
Ateles
Pithecia
Hominidae
Homo
Platyrrhini
Cercopithecoidea
Theropithecus
Pongo
Piliocolobus
Cebus
Saimiri
Homunculus
Oreopithecus
Trachypithecus
P.paniscus
Presbytis
Aotus
P.troglodytes
Nasalis
Callicebus
Aegyptopithecus
Mandrillus
Miopithecus
Colobus
Papio
Macaca
Dolichocebus
Lophocebus
Cercocebus
Chlorocebus
Erythrocebus
Cercopithecus
Parapithecus
Gorilla
Callithrix
bgPC3 11.0%
bgPC1 59.0%
Crown anthropoid LCA
Crown platyrrhine LCA
Crown catarrhine LCA
Crown hominoid LCA

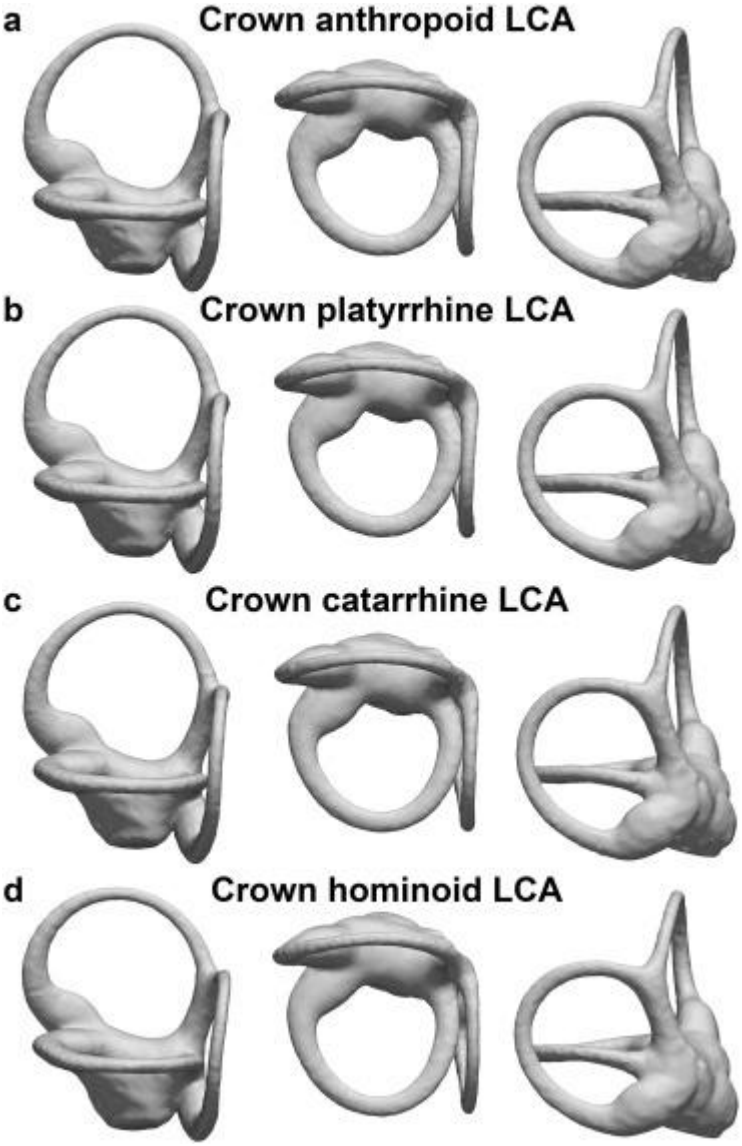
a
Crown anthropoid LCA
b
Crown platyrrhine LCA
c
Crown catarrhine LCA
d
Crown hominoid LCA

1270

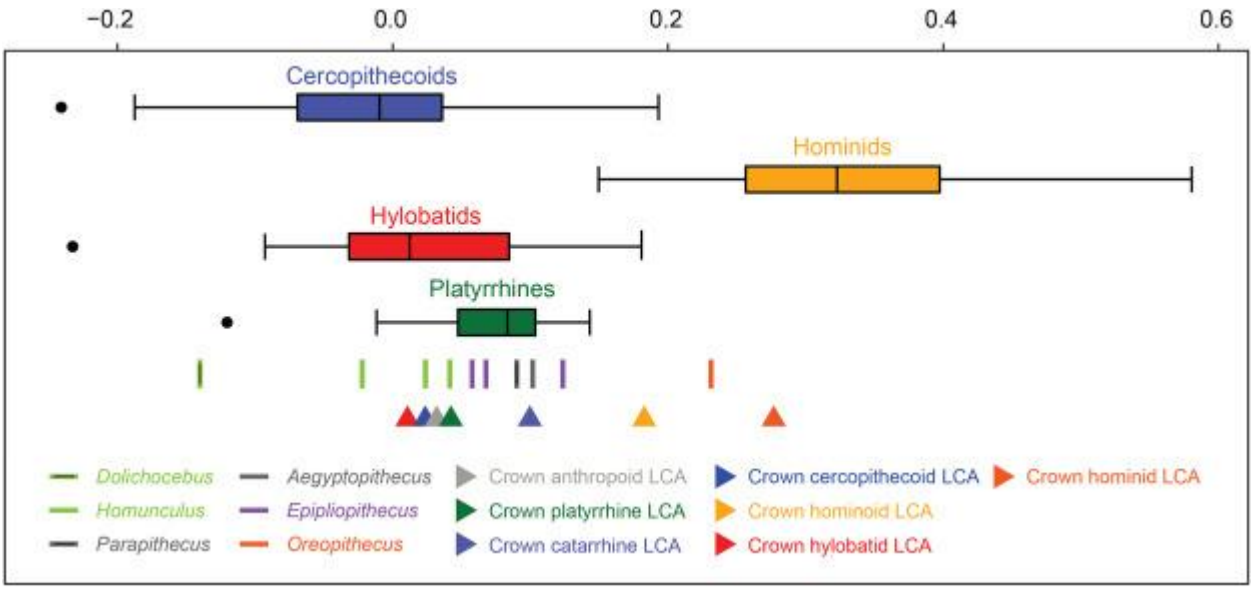
−0.2
0.0
0.2
0.4
0.6
Cercopithecoids
Hominids
Hylobatids
Platyrrhines
Dolichocebus
Homunculus
Parapithecus
Aegyptopithecus
Epipliopithecus
Oreopithecus
Crown anthropoid LCA
Crown platyrrhine LCA
Crown catarrhine LCA
Crown cercopithecoid LCA
Crown hominoid LCA
Crown hylobatid LCA
Crown hominid LCA

1271

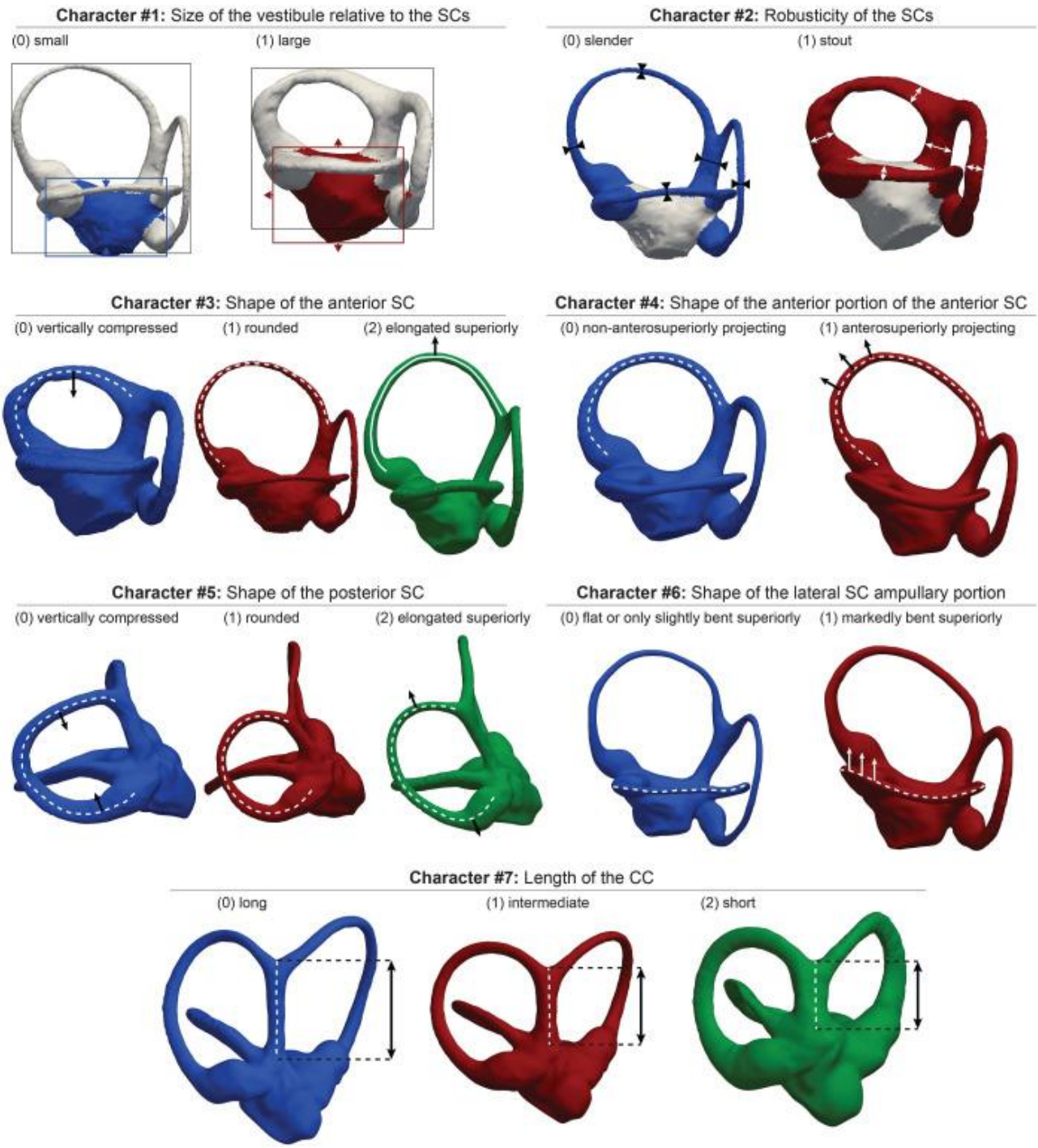
Character #1: Size of the vestibule relative to the SCs
(0) small
(1) large
Character #2: Robusticity of the SCs
(0) slender
(1) stout
Character #3: Shape of the anterior SC
(0) vertically compressed
(1) rounded
(2) elongated superiorly
Character #4: Shape of the anterior portion of the anterior SC
(0) non-anterosuperiorly projecting
(1) anterosuperiorly projecting
Character #5: Shape of the posterior SC
(0) vertically compressed
(1) rounded
(2) elongated superiorly
Character #6: Shape of the lateral SC ampullary portion
(0) flat or only slightly bent superiorly
(1) markedly bent superiorly
Character #7: Length of the CC
(0) long
(1) intermediate
(2) short

1272

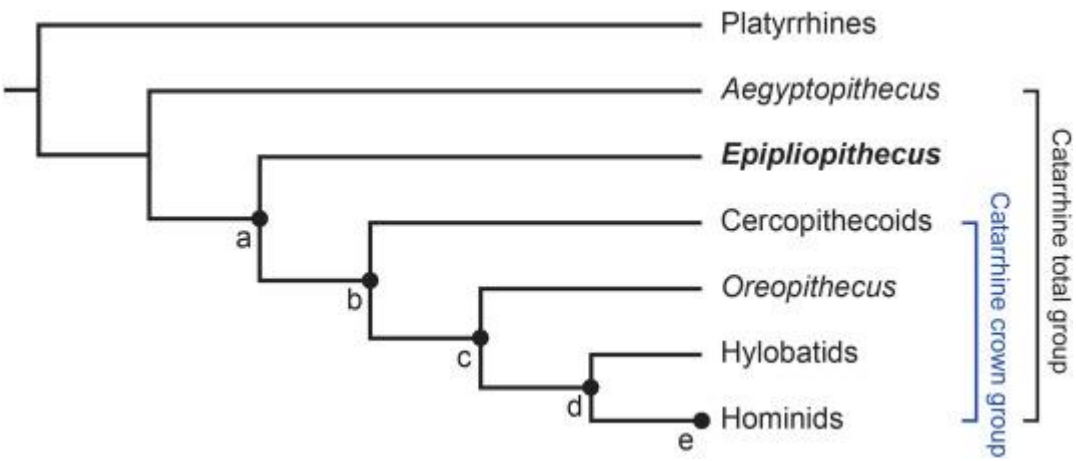
Platyrrhines
Aegyptopithecus
Epipliopithecus
Cercopithecoids
Oreopithecus
Hylobatids
Hominids
a
b
c
d
e
Catarrhine total group
Catarrhine crown group

1273